РОССИЙСКИЙ ГОСУДАРСТВЕННЫЙ ПЕДАГОГИЧЕСКИЙ УНИВЕРСИТЕТ им. А. И. ГЕРЦЕНА
HERZEN STATE PEDAGOGICAL UNIVERSITY of RUSSIA

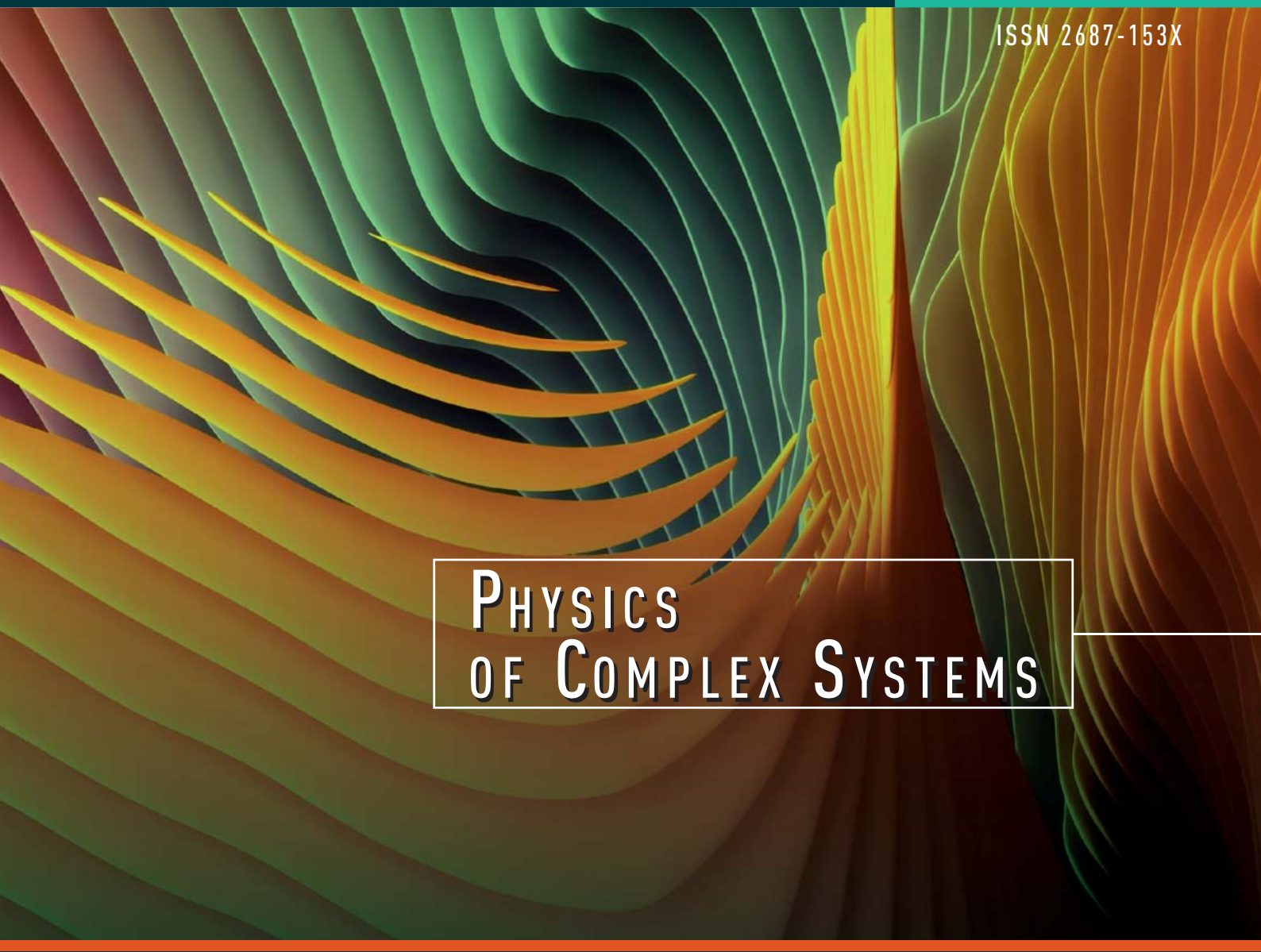

ISSN 2687-153X

Physics of Complex Systems

Т. 4 № 2 2023

Vol. 4 No. 2 2023

Herzen State Pedagogical University of Russia

ISSN 2687-153X (online)
physcomsys.ru
https://www.doi.org/10.33910/2687-153X-2023-4-2
2023. Vol. 4, no. 2

PHYSICS OF COMPLEX SYSTEMS

Mass Media Registration Certificate El No. FS77-77889, issued by Roskomnadzor on 10 February 2020
Peer-reviewed journal
Open Access
Published since 2020
4 issues per year

Publishing house of Herzen State Pedagogical University of Russia
48 Moika Emb., Saint Petersburg 191186, Russia
E-mail: izdat@herzen.spb.ru
Phone: +7 (812) 312-17-41

Data size 3,89 Mbyte
Published at 09.06.2023

Editors of the English text *M. V. Bumakova, I. A. Nagovitsyna*
Corrector *E. V. Novoseltseva*
Cover design by *O. V. Rudneva*
Layout by *A. M. Khodan, L. N. Kliuchanskaya*

CONTENTS

Condensed Matter Physics. Dielectrics

UDC 537.9

EDN ZFBEBQ
https://www.doi.org/10.33910/2687-153X-2023-4-2-47-52

Thermoactivational spectroscopy of polyethylene polymer films with an ethylene-vinyl acetate copolymer

M. F. Galikhanov[1], E. A. Karulina[2], E. E. Fomicheva[3], T. V. Reztsov✉[2]

[1] Kazan National Research Technological University, 68 Karl Marx Str., Kazan 420015, Russia
[2] Herzen State Pedagogical University of Russia, 48 Moika Emb., Saint Petersburg 191186, Russia
[3] Military Space Academy named after A. F. Mozhaysky, 13 Zhdanovskaya Emb., Saint Petersburg 197198, Russia

Authors

Mansur F. Galikhanov, ORCID: 0000-0001-5647-1854, e-mail: galikhanovMF@corp.knrtu.ru

Elena A. Karulina, ORCID: 0000-0001-9604-4769, e-mail: karulina@mail.ru

Elena E. Fomicheva, ORCID: 0000-0002-9402-5246, e-mail: e.e.fomicheva@gmail.com

Tikhon V. Reztsov, ORCID: 0000-0003-2025-0579, e-mail: sunnyundeadjuvati@icloud.com

For citation: Galikhanov, M. F., Karulina, E. A., Fomicheva, E. E., Reztsov, T. V. (2023) Thermoactivational spectroscopy of polyethylene polymer films with an ethylene-vinyl acetate copolymer. *Physics of Complex Systems*, 4 (2), 47–52. https://www.doi.org/10.33910/2687-153X-2023-4-2-47-52 EDN ZFBEBQ

Received 30 March 2023; reviewed 21 April 2023; accepted 21 April 2023.

Funding: This study was supported by the Ministry of Education of the Russian Federation as part of the state-commissioned assignment (project No. VRFY-2023-0005).

Abstract. The article reports the results of the study of polymer films based on the blend of high-pressure polyethylene (LDPE) and the ethylene-vinyl acetate copolymer (EVA, sevilen). The films were investigated with thermally stimulated depolarization. It is noted that one maximum is observed on the temperature dependences of the depolarization currents obtained for samples with different sevilen content. It is assumed that this maximum corresponds to the dipole-segmental relaxation that occurs in high-pressure polyethylene. Calculation results of activation energies corresponding to this process allow us to conclude that an increase in the proportion of EVA in the blend leads to an increase in the dipole-segmental mobility and, as a consequence, to an increase in the flexibility of the polymer.

Keywords: polyethylene, ethylene-vinyl acetate copolymer, thermally stimulated depolarization, thermoactivational spectroscopy, dipole-segmental relaxation

Introduction

Today, new ways of using polyolefins in various fields of technology are emerging. One of the areas of polymer dielectrics application is the creation of electrets. Electrets are dielectrics which create a strong electrostatic field in the surrounding space as a result of their polarization. They are used in the production of electroacoustic and electromechanical transducers and electret air filters. Also, electrets are used in medicine and industrial applications as active packaging materials, etc. This can be achieved by changing the structure of the polymer or the composition of the copolymer matrix.

One typical representative of polyolefins is polyethylene, e.g., high pressure polyethylene (LDPE). It is a non-polar polymer that has fairly good dielectric properties due to the structure of its macromolecules. It is characterized by a low permittivity, high electrical resistivity, and high dielectric strength.

However, according to (Burda 2013) and (Gorokhovatskij 2009), LDPE has a rather short electret state lifetime. Nevertheless, it should be noted that this material has good mechanical properties.

It is also relatively cheap to manufacture and, therefore, is widely used in technology, medicine and other sectors. Hence, increasing the stability of the electret state in LDPE films holds promise.

In recent years, structural parameters and external conditions that affect electret properties of polyethylene have been actively studied (Galikhanov et al. 2009; 2017; Shkuro et al. 2012).

Today, targeted improvement of the physicochemical properties of a polymer is achieved through using the modification method. It is based on the creation of polymer-polymer compositions. One of the frequently used polymer blends in the manufacturing of such compositions is the combination of polyethylene and an ethylene-vinyl acetate copolymer. Mixing different types of polymers with sevilen is widely used to change mechanical and electrical properties of polymers (Ableev et al. 2016; Baulin et al. 2015; Mishak et al. 2007).

EVA (sevilen) is a polar polymer whose polarity is determined by the presence of vinyl acetate. It is known that as the content of vinyl acetate increases, the flexibility and strength of sevilen improve at low temperatures. This makes it an appropriate material for active packaging for frozen foods (Stepanov et al. 2015). Elastic electrets can be used not only as active packaging, but also in soft electronics, such as pulse wave or heartbeat sensors and tactile control devices (Baulin et al. 2015; Mishak et al. 2007).

Considering the relevance of studies in elastic electret polymers, an ethylene-vinyl acetate copolymer may turn out to be an appropriate material. Despite the fact that the electret properties of savilene have been thoroughly described (Galikhanov 2006; Galikhanov, Budarina 2002), it is still not completely clear how the percentage of EVA in the structure of the LDPE copolymer affects its electrophysical parameters.

In this regard, the purpose of this work is to investigate the effect of the percentage of EVA in the composite modification with LDPE on the electrical properties of LDPE.

Samples and research methods

The study focused on the blends of high-pressure polyethylene with an ethylene-vinyl acetate copolymer of different ratio of components. The film samples have a thickness of about 300 μm.

The blending of polymers is carried out on laboratory microrollers at a temperature of 130 ± 5 °C. The blending time is 3 minutes. The films are prepared by pressing at a temperature of 170 ± 5 °C. The holding time under pressure is 5 minutes. Samples of blends of LDPE and EVA are provided by the Kazan National Research Technological University.

The method of thermally stimulated depolarization (TSD) is chosen as the main research method. The essence of the method lies in the polarization of the sample during its cooling and further measurement of currents when the samples are heated. The polarization of the sample is carried out at a temperature above the glass transition temperature (Sazhin et al. 1986), followed by a temperature decrease with turned on field. In this case, the orientation of the dipoles is frozen. Heating the sample leads to an increase in the molecular mobility of the dipoles. As a result, while the sample is heated, a depolarization current flows through it. This current corresponds to relaxation transitions, which appear as maxima in the depolarization spectrum (Gorokhovatskij, Bordovskij 1991; Sessler 1983).

In the study, thermally stimulated currents are measured on a TSC-II (Setaram). Resolution for measuring current is 10^{-16} A. Operating temperatures range is from –150 °C to 250 °C. Temperature measurement error is 0.1 °C. The samples are polarized by the contact method by applying an electric field of 100 V/mm for 2 minutes at a temperature of 40 °C, after which they are cooled at a rate of 2 °C/min to 0 °C in the applied field. The studies are carried out at heating rates of 3 °C/min, 7 °C/min, 9 °C/min.

The activation energy is calculated by varying the heating rate (Gorokhovatskij, Bordovskij 1991). Depolarisation curves are obtained at two sample heating rates. Based on them, the energy distribution functions of electrically active defects are constructed, which make it possible to estimate the activation energy.

Experimental results and discussion

The TSD spectra show one process (Fig. 1) represented as a maximum. Its position depends on the ratio of components in the blend. When increasing the EVA percentage, the maximum shifts to lower temperatures and its height decreases. The dependence of the temperature position of the maximum peak on the EVA percentage is described by a linear dependence (Fig. 2).

 https://www.doi.org/10.33910/2687-153X-2023-4-2-47-52

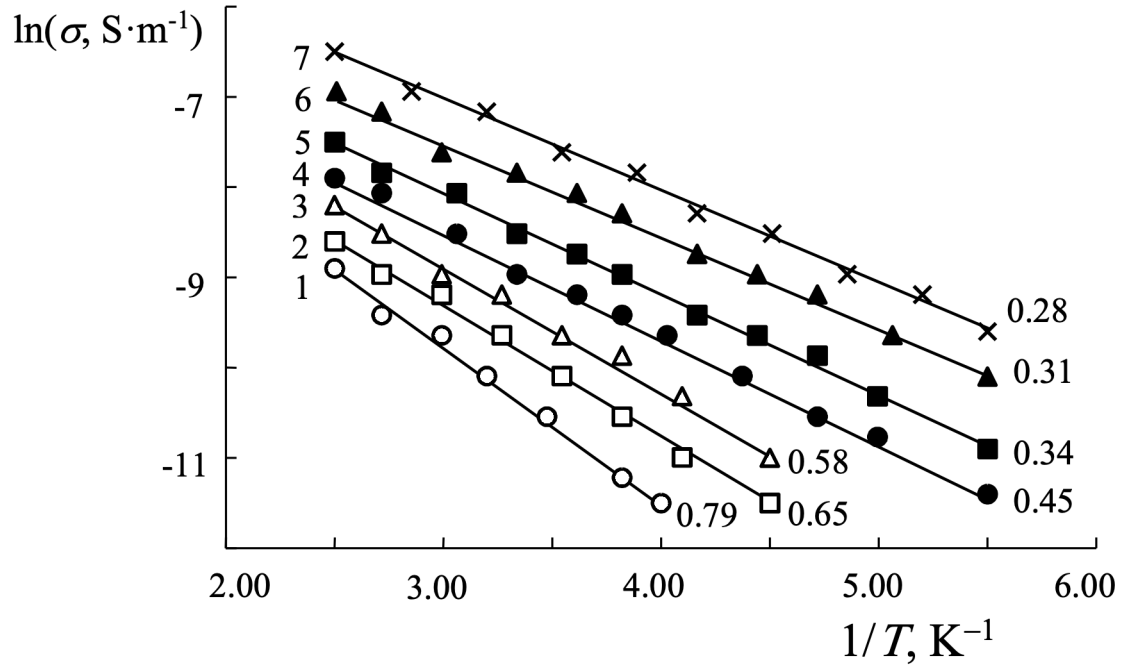

Fig. 1. The temperature dependences of the depolarization currents obtained for samples of the LDPE–EVA with different EVA percentages

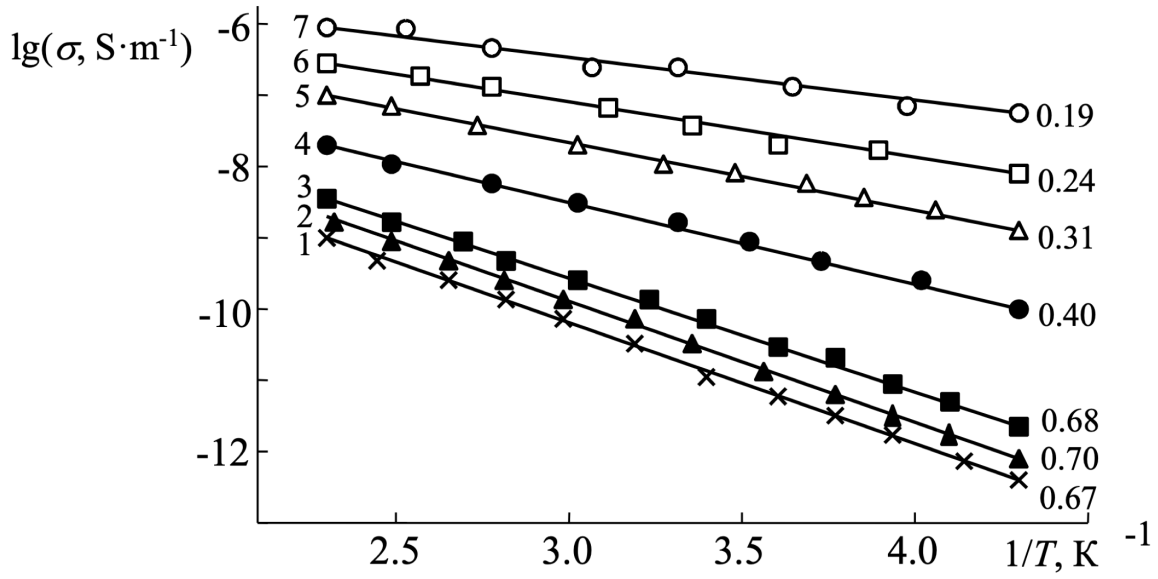

Fig. 2. The dependence of the temperature position of the maximum on the EVA percentage in the blend

It is known (Ellis, Smith 2008) that dipole-segmental relaxation (α-relaxation) is observed in polyethylene between 40 and 50 °C. As is said before, polyethylene is a nonpolar polymer. However, it contains polar carbonyl groups C = O and the dielectric relaxation occurs due to them (Sessler 1983).

Extrapolation of the straight line describing the shift of the peak position to the region where the EVA percentage tends to zero indicates a temperature around 40 °C (Fig. 2). It can be assumed that the maximum observed in Fig. 1 corresponds to the process of charge accumulation and relaxation occurring in polyethylene. An increase in the EVA percentage in the blend leads to a shift of this process to lower temperatures. In this case, the number of relaxers in polyethylene decreases and their mobility is facilitated.

The area under the plot of current versus time for the TSD spectra is calculated. It corresponds to the charge released during relaxation. In the case of dipole-segmental relaxation, this is evidence in favor of the rotation of chain segments. The decrease in the peak area indicates the decrease in the amount of relaxers in the blend and also confirms that polyethylene is responsible for the presence of the peak in the TSD spectrum (Fig. 3).

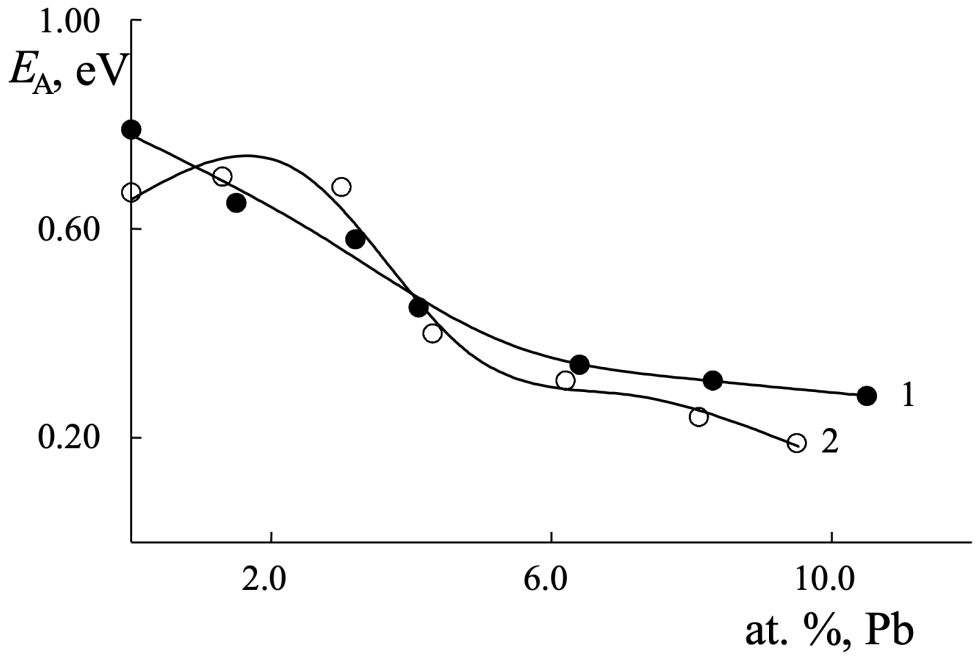

Fig. 3. The dependence of the area under the graphics on the EVA percentage in the blend

The process observed on the depolarization currents spectra has a thermally activated origin. As the sample heating rate increases, the maximum shifts towards higher temperatures (Fig. 4).

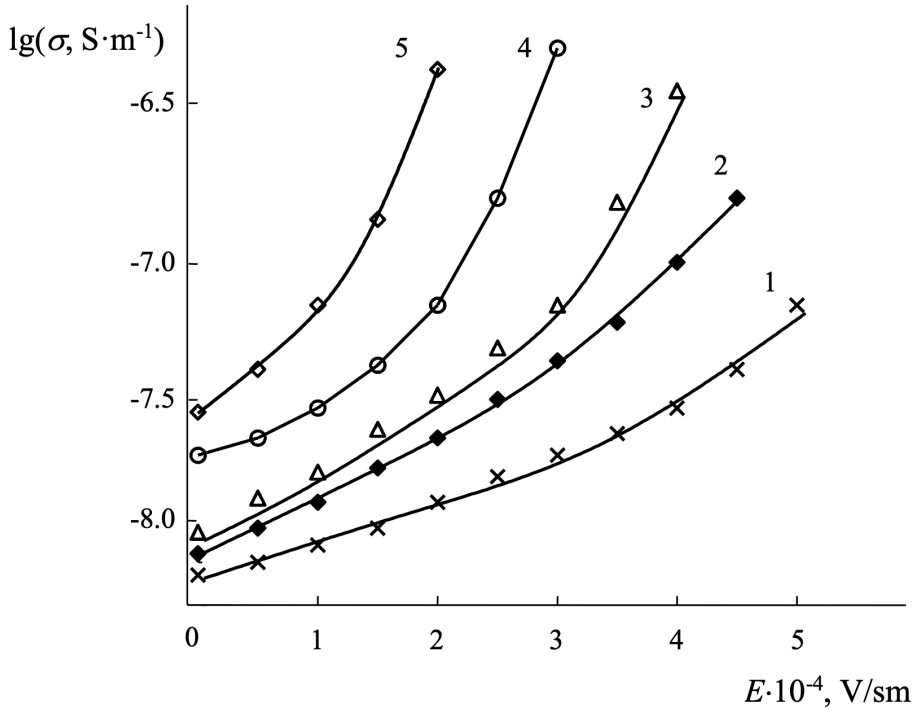

Fig. 4. The temperature dependences of the depolarization currents obtained for samples with the same EVA percentage (70%) but at different heating speeds: 1—7 °C/min, 2—9 °C/min

 https://www.doi.org/10.33910/2687-153X-2023-4-2-47-52

By measuring the depolarization currents for several heating rates, the activation energy corresponding to electrically active defects in these samples can be estimated. The activation energies calculated by the method of varying the heating rate are shown in Table 1.

Table 1. The dependence of the activation energy on the EVA percentage in the copolymer

The EVA percentage, %	The activation energy, eV
30	0.52
40	0.50
50	0.50
60	0.46
70	0.45
80	0.35
90	0.33

With an increase in the precentage of EVA in the blend, a slight decrease in the values of the activation energy is observed. This fact indicates that the mobility of the chain segments is facilitated and the polymer becomes more flexible.

It is known from (Ellis, Smith 2008) that with a change in the degree of crystallinity of the polymer, the maximum temperature of the peak corresponding to α-relaxation shifts at a practically constant activation energy. The behavior of the peak in the TSD spectra of the blend of LDPE and EVA is similar to the data analyzed in (Sazhin et al. 1986). This may be another confirmation that α-relaxation is the reason for the appearance of this maximum in the TSD spectra.

Conclusions

The study demonstrates that there is one maximum in the spectra of thermally stimulated depolarization of LDPE and EVA blends. Its presence may be associated with the relaxation processes occurring in polyethylene. The depolarization current maximum shifts to the region of lower temperatures with an increase in the EVA percentage. In this case, the area of the maximum decreases.

It has been suggested that this process is associated with dipole-segmental relaxation in polyethylene due to the presence of carbonyl groups in the crystalline region of the polymer. A decrease in the peak area in the TSD spectrum with an increase in the percentage of EVA in the blend confirms that the process occurring in polyethylene is the reason for the appearance of the maximum.

It has been established that the activation energy corresponding to this process decreases with an increase in the EVA percentage in the blend. Therefore, an increase in the EVA percentage facilitates dipole-segmental mobility and the polymer becomes more flexible. Blends of increased flexibility may find an application in production processes that use flexible polymers.

Conflict of Interest

The authors declare that there is no conflict of interest, either existing or potential.

Author Contributions

All the authors discussed the final work and took part in writing the article.

References

Ableev, R. I., Baranets, I. V., Kurlyand, S. K. et al. (2016) Vliyanie sopolimera etilena i vinilatsetata na formirovanie strukturno-tekhnologicheskikh svojstv olefinovykh termoelastoplastov [Effect of copolymer of ethylene and vinyl acetate on formation of structure and processing properties of olefin TPV]. *Kauchuk i Rezina*, 5, 12–17. (In Russian)

Baulin, A. A., Kalandin, A. V., Kudryavtseva, N. A. (2015) Povyshenie stojkosti k rastreskivaniyu kompozitsii polietilena nizkogo davleniya [Improving the cracking resistance of a low-pressure polyethylene composition]. *Plasticheskie massy*, 9-10, 21–25. (In Russian)

Burda, V. V. (2013) *Relaksatsiya elektretnogo sostoyaniya v biorazlagaemykh kompozitnykh polimernykh plenkakh na osnove polietilena vysokogo davleniya s binarnym napolnitelem [Relaxation of the electret state in biodegradable composite polymer films based on high-density polyethylene with binary filler]. PhD dissertation (Physics).* Saint Petersburg, Herzen State Pedagogical University of Russia, 104 p. (In Russian)

Ellis, B., Smith, R. (ed.). (2008) *Polymers. A property database*. 2nd ed. Boca Raton: CRC Press, 1052 p. https://doi.org/10.1201/9781420005707 (In English)

Galikhanov, M. F. (2006) Izuchenie koronoelektretov na osnove smesej polietilena s sopolimerami etilena s vinilatsetatom [Investigation of corona electrets based on a mixture of polyethylene with ethylene-vinyl acetate copolymers]. *Materialovedenie: nauchno-tekhnicheskij zhurnal — Materials Sciences Transactions*, 12, 30–34. (In Russian)

Galikhanov, M. F., Budarina, L. A. (2002) Koronoelektrety na osnove polietilena i sopolimerov etilena s vinilatsetatom [Corona electrets based on polyethylene and ethylene-vinyl acetate copolymers]. *Plasticheskie massy*, 1, 40–42. (In Russian)

Galikhanov, M. F., Deberdeev, T. R., Karimov, I. A. et al. (2017) Vliyanie strukturnykh parametrov polietilena na ego elektretnye svojstva [Influence of structural parameters of polyethylene on its electret properties]. *Plasticheskie massy*, 1-2, 14–17. (In Russian)

Galikhanov, M. F., Zhigaeva, I. A., Minakhmetova, A. K. et al. (2009) Elektretnye svojstva kompozitsij sopolimerov etilena s vinilatsetatom krakhmalom [Electret properties of compositions of copolymers of ethylene with vinyl acetate starch]. *Izvestia Rossijskogo gosudarstvennogo pedagogicheskogo universiteta im. A. I. Gertsena — Izvestia: Herzen University Journal of Humanities & Sciences*, 79, 115–119. (In Russian)

Gorokhovatskij, I. Yu. (2009) *Issledovanie stabil'nosti elektretnogo sostoyaniya v kompozitnykh plenkakh na osnove polietilena vysokogo davleniya s nanorazmernymi vklyucheniyami dvuokisi kremniya [Investigation of the stability of the electret state in composite films based on high-pressure polyethylene with nanosized inclusions of silicon dioxide]. PhD dissertation (Physics).* Saint Petersburg, Herzen State Pedagogical University of Russia, 137 p. (In Russian)

Gorokhovatskij, Yu. A., Bordovskij, G. A. (1991) *Termoaktivatsionnaya tokovaya spektroskopiya vysokoomnykh poluprovodnikov i dielektrikov [Thermoactivational current spectroscopy of high-resistance semiconductors and dielectrics].* Moscow: Nauka Publ., 248 p. (In Russian)

Mishak, V. D., Seminog, V. V., Ostapyuk, S. M. et al. (2007) Vliyanie dobavok sopolimera etilena s vinilatsetatom na fiziko-mekhanicheskie svojstva kompozitov na osnove vtorichnogo polietilena i dispersnoj rezinovoj kroshki [Influence of additives of an ethylene-vinyl acetate copolymer on the physical and mechanical properties of composites based on secondary polyethylene and dispersed crumb rubber]. *Polimernyj zhurnal*, 29 (4), 320–327. (In Russian)

Sazhin, B. I., Lobanov, A. M., Romanovskaya, A. S. et al. (1986) *Elektricheskie svojstva polimerov*. 3rd ed. Leningrad: Khimiya Publ., 224 p. (In Russian)

Sessler, G. M. (1983) *Elektrety [Electrets]*. Moscow: Mir Publ., 487 p. (In Russian)

Shkuro, A. E., Glukhikh, V. V., Mukhin, N. M. et al. (2012) Vliyanie soderzhaniya sevilena v polimernoj matritse na svojstva drevesno-polimernykh kompozitov [Influence of savilene content in the polymer matrix on the properties of wood-polymer composites]. *Vestnik Kazanskogo tekhnologicheskogo universiteta*, 15 (17), 92–95. (In Russian)

Stepanov, G. V., Navrotskii, V. A., Gaidadin, A. N., Ermolin, A. S. (2015) Termoplastichnye elastomery na osnove sopolimera etilena s vinilatsetatom [Thermoplastic elastomers based on copolymers of ethylene with vinyl acetate]. *Izvestiya Volgogradskogo gosudarstvennogo tekhnicheskogo universiteta*, 4 (159), 101–106. (In Russian)

Condensed Matter Physics. Dielectrics

UDC 537.9

EDN YGEOSE
https://www.doi.org/10.33910/2687-153X-2023-4-2-53-58

Complex dielectric permittivity of films in the infra-low frequency range as studied by relaxation maps of thermally stimulated currents

E. A. Volgina✉[1]

[1] Herzen State Pedagogical University of Russia, 48 Moika Emb., Saint Petersburg 191186, Russia

Author

Elena A. Volgina, ORCID: 0000-0002-1536-5841, e-mail: volgina.elena.1999@mail.ru

For citation: Volgina, E. A. (2023) Complex dielectric permittivity of films in the infra-low frequency range as studied byrelaxation maps of thermally stimulated currents. *Physics of Complex Systems*, 4 (2), 53–58. https://www.doi.org/10.33910/2687-153X-2023-4-2-53-58 EDN YGEOSE

Received 13 March 2023; reviewed 14 April 2023; accepted 14 April 2023.

Funding: This study was supported by the Ministry of Education of the Russian Federation as part of the state-commissioned assignment (project No. VRFY-2023-0005).

Abstract. The paper shows the possibility of interpreting the results of thermal activation spectroscopy of PVDF polymer films obtained by thermally stimulated currents of fractional polarization using the concepts of low-frequency dielectric spectroscopy. The paper presents the results of the study of temperature-frequency dependences of the components of complex dielectric permittivity in PVDF films with different degrees of orientation, polymorphic composition and pore percentage. It also provides the parameters of electrically active defects responsible for relaxation processes in the temperature range under study.

Keywords: porous films, polyvinylidenftoride, thermactivational spectroscopy, dielectric spectroscopy, dielectric parameters

Introduction

The methods of thermal activation analysis have been actively used since the end of the 20th due to fairly simple experimental technology combined with great processing capabilities of experimental results. One of the methods of thermal activation analysis is the method of thermally stimulated currents in fractional polarization (TSC-FP). It allows to recalculate the results obtained by dielectric spectroscopy (DS) in the infralow frequencies of the order of 10^{-2}–10^{-5} Hz with significantly less time compared to the traditional method of dielectric spectroscopy.

In this paper, polyvinylidene fluoride (PVDF) films with different polymorphic composition and pore percentage were studied by the method of thermally stimulated fractional polarization currents.

The properties of PVDF, including electrophysical ones, are largely determined by various modifications of its crystal phase (α-, β-, γ- modifications) (Kochervinskii 1996). A pronounced piezoelectric effect is manifested in a PVDF film containing a large amount of the polar β- phase. The presence of pores in such materials can significantly expand the scope of their application. The formation of the polar phase and pores is possible due to orientation extraction carried out at certain tempretures.

The change in the structure also significantly affects the dielectric properties of this polymer dielectric permittivity and dielectric losses. This is explained by the change in the dipole moment of the monomer link and the relaxation time. Therefore, dielectric properties can be used as a characteristic of a rather complex polymorphic polymer structure (Kochervinskii 1996).

Materials and methods

The paper investigated porous films made from PVDF granules of the commercial brand Kynar-720 (Atofina Chemicals, USA), with a molecular weight of M_w = 190000 g·mole^{-1} and the melting point 168 °C.

The films were obtained in a four-stage process: polymer melt extrusion, isometric annealing, uniaxial stretching and thermal fixation (Elyashevich et al. 1997). The first stage of film formation is characterized by the parameter λ- multiplicity of the die drawing. This stage affects the structure of the studied samples and the degree of orientation. The paper (Gerasimov et al. 2020) shows that at low values of the multiplicity of the die extraction (λ < 20), a weakly oriented spherulite structure prevails in the crystal phase of the samples. In samples with λ > 20, an oriented lamellar structure is formed. In this paper, films with λ = 29 and λ = 15 were studied.

Annealing of the extruded films under isometric conditions was carried out at a temperature close to the melting temperature of 167 °C.

At the stage of uniaxial stretching, both the formation of pores and the structural α→β transition occur. The polymorphic composition of the crystal structure (N) and the total porosity (P) are determined by the orientation parameter *ε*—the degree of orientation extraction.

To give stability to the formed structure after stretching, the films were thermofixed for 1 hour at a temperature of T = 100 °C (Gerasimov et al. 2022).

The total proportion of pores in the polymer volume was calculated by the formula:

$$P = \left[\left(\rho - \rho_0 \right) / \rho \right] \cdot 100\%, \quad (1)$$

where ρ is the density of the extruded film, ρ_0 is the density of the porous film.

The content of the β-phase in various samples was determined by X-ray diffraction analysis. The amount of β-phase of porous films was determined by the formula:

$$N = \frac{\beta}{\alpha + \beta} \cdot 100\%. \quad (2)$$

Table 1 shows the parameters P and N for all the samples under study.

Table 1. Parameters of the studied samples

λ	ε, %	P, %	N, %
15	0	0	0
29	0	0	0
	30	13	26
	50	19	33

The samples were examined in the temperature range from 0–70°C in a helium atmosphere using TSC II by Setaram, France. The current was measured using a Keithley electrometer with a resolution of 10^{-16} A.

The method of thermally stimulated currents in the mode of a fractionally polarized dielectric was proposed by Lacabanne and Chatain. Fractional polarization is achieved by polarizing the sample for 2 minutes (τ_b) at a temperature of 40 °C (T_b). This is followed by cooling the sample to 35 °C (T_d) (usually T_d differs from T_b by only a few degrees) and follow-up depolarization at T_d for 1 minute (τ_d). During depolarization, the external field is turned off and the sample is shorted. Later, the sample is cooled to an initial temperature of 0°C (T_0), after which it is linearly heated and the thermally stimulated short-circuit current is registered. To obtain the energy spectrum of relaxers (charge traps, the described measurement procedure must be repeated many times each time increasing the temperature with a certain step T_b and T_d (other conditions of polarization and depolarization remain unchanged). Figure 1 illustrates the measurement procedure of the TSC-FP method.

 https://www.doi.org/10.33910/2687-153X-2023-4-2-53-58

Due to partial depolarization of the sample before each subsequent heating, it is possible to narrow the interval of activation energy of relaxators (traps for charge carriers). They participate in the formation of a thermally stimulated current in the linear heating section.

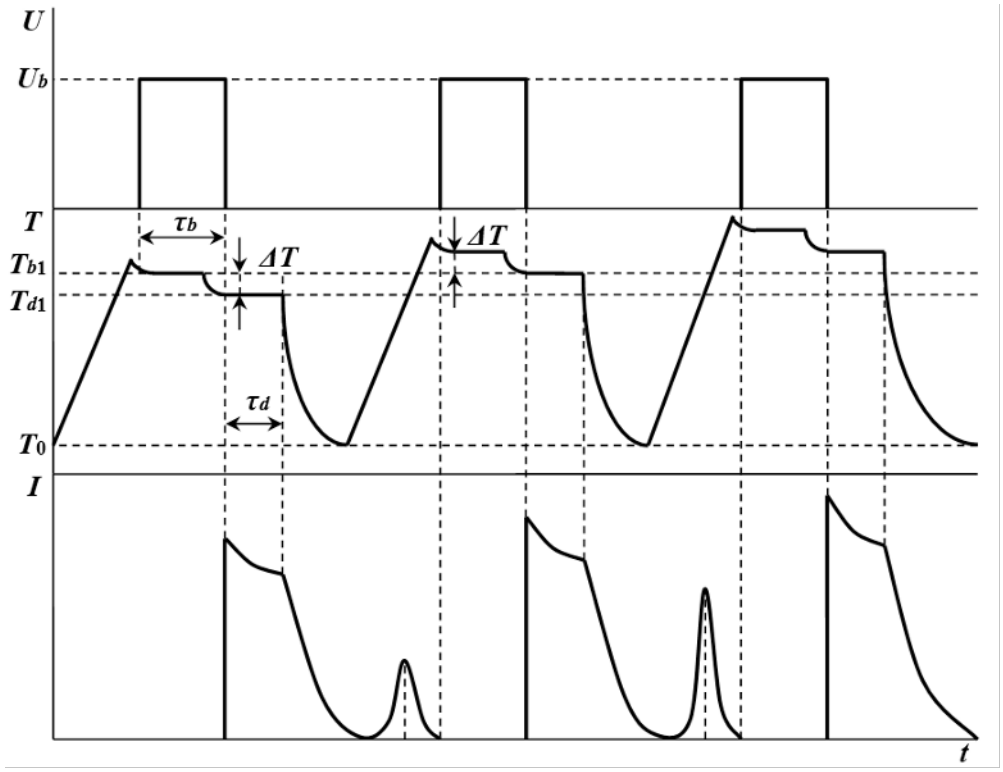

Fig. 1. Operating mode of the TSC-FP method. TSC-TS. U_b, T_b, and τ_b—voltage, temperature and relaxation time; T_d, and τ_b —temperature and time of pre–depolarization; ΔT—step of change of polarization and depolarization temperatures

The resulting current dependence is described by the expression:

$$j(T) \simeq j_0 e^{-\frac{W}{kT}}. \tag{3}$$

In (van Turnhout 1975), van Turnhout showed a quantitative relationship between experimentally obtained TSC-FP spectra and low-frequency dielectric loss spectra. The following relation illustrates the relationship between dielectric losses (ε″) and depolarization current (J(t)):

$$\varepsilon'' = \frac{J(t)}{A 2\pi\varepsilon_0 FE} \quad , \tag{4}$$

where A is the sample area, E is the polarization field strength, ε_0 is the dielectric constant and F is the effective frequency of the experiment. The effective frequency can be determined by the formula:

$$F = \frac{E_a}{2\pi s R T^2} \quad , \tag{5}$$

where s is the inverse heating rate, E_a is the activation energy.

Each TSC scan represents a convoluted spectrum of the dielectrically active relaxations excited between T_b and T_0. It has been shown that the integrated peak area of a given transition is related to the strength of the transition defined by the dielectric increment (van Turnhout 1975)

$$\Delta\varepsilon = \frac{1}{E\varepsilon_0}\int_{t_0}^{\infty}\frac{J}{A}dt \quad , \tag{6}$$

where t_o to infinity is the time-span which covers the entire transition measured upon reheating at a constant rate, and the dielectric increment is defined as:

$$\Delta\varepsilon = \varepsilon'_{\infty} - \varepsilon'_{0} \quad , \tag{7}$$

where ε' is the dielectric constant at high frequency (or low temperature), and ε" is the dielectric constant at low frequency (or high temperature). Since the TSC experiment is obtained at a constant heating rate, temperature was converted to time in eq. (6).

Results

Figures 2 and 3 show the results of the dependence of dielectric losses in the infra-low frequency region on temperature for samples λ = 29 and λ = 15.

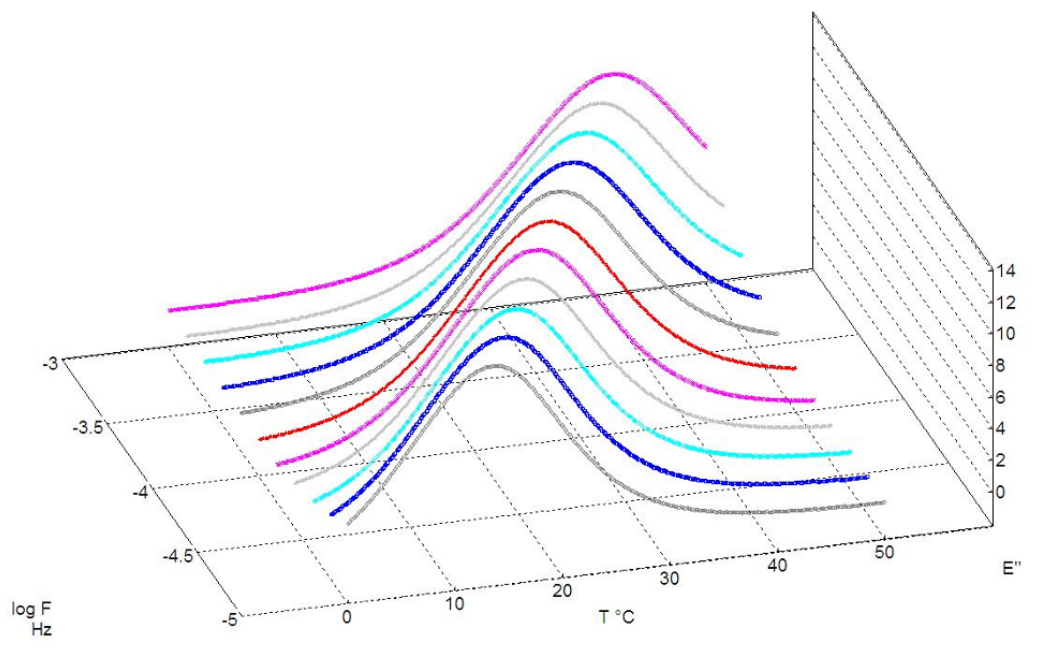

Fig. 2. Temperature-frequency dependence of dielectric losses for λ = 15

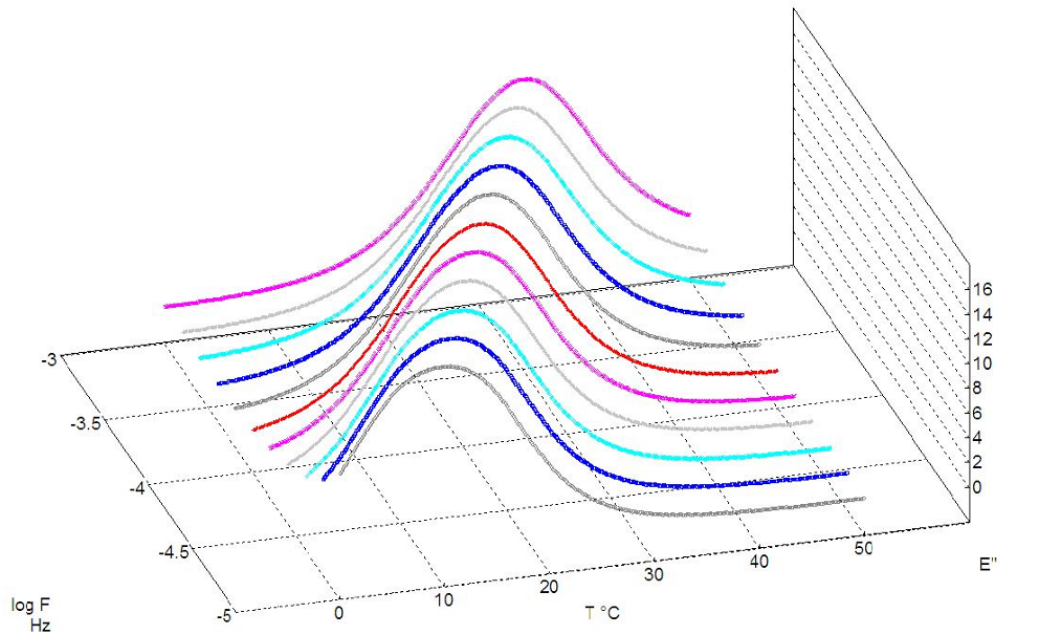

Fig. 3. Temperature-frequency dependence of dielectric losses for λ = 29

 https://www.doi.org/10.33910/2687-153X-2023-4-2-53-58

The analysis of the obtained curves shows the presence of one maximum in the temperature range from 0 ˚C to 50 ˚C. The construction of the dependence of dielectric losses on temperature at one frequency shows that a change in the supramolecular structure shifts the peak of dielectric losses to the region of lower temperatures (Fig. 4).

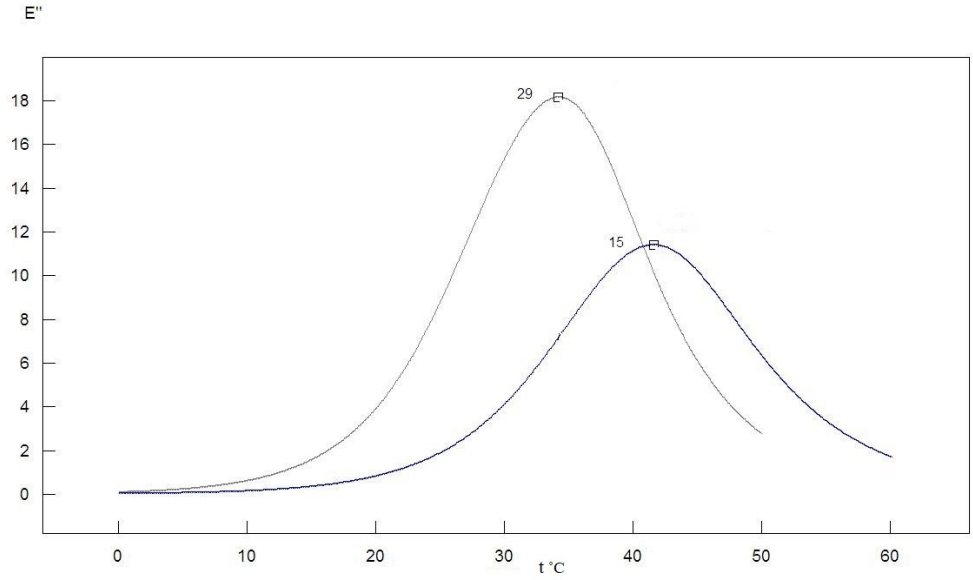

Fig. 4. Dependence of dielectric losses on temperature at one frequency of 10^{-3} Hz for samples λ = 15 and λ = 29

The paper also analyzes the dependences of dielectric losses on temperature in samples with different polymorphic composition (different percentages of β-phase) and different percentages of pores (Fig. 5). The activation energy in the samples with ε = 30% in its values approximately coincides with the original films —0.94 eV. In the samples with a large amount of β-phase (ε = 50%), there is a noticeable decrease in the activation energy to 0.83 eV (Gerasimov et al. 2022), which leads to a noticeable shift of the peak of dielectric losses to the low-temperature region.

It can be seen from the diagrams (Fig. 6) that with an increase in the degree of orientation drawing, the angle formed by the abscissa axis and the line connecting the center of the circle increases, which indicates a change in the distribution of relaxation times in the studied films (Gusev 2008).

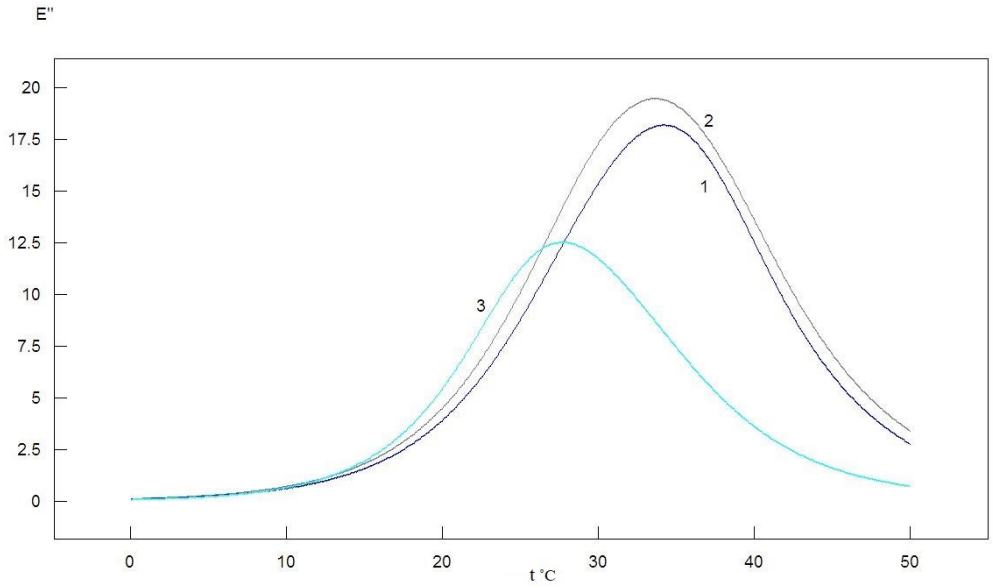

Fig. 5. Dependence of dielectric losses on temperature at one frequency of 10^{-3} Hz for samples λ = 29, 1—ε = 0, 2—ε = 30%, 3—ε = 50%

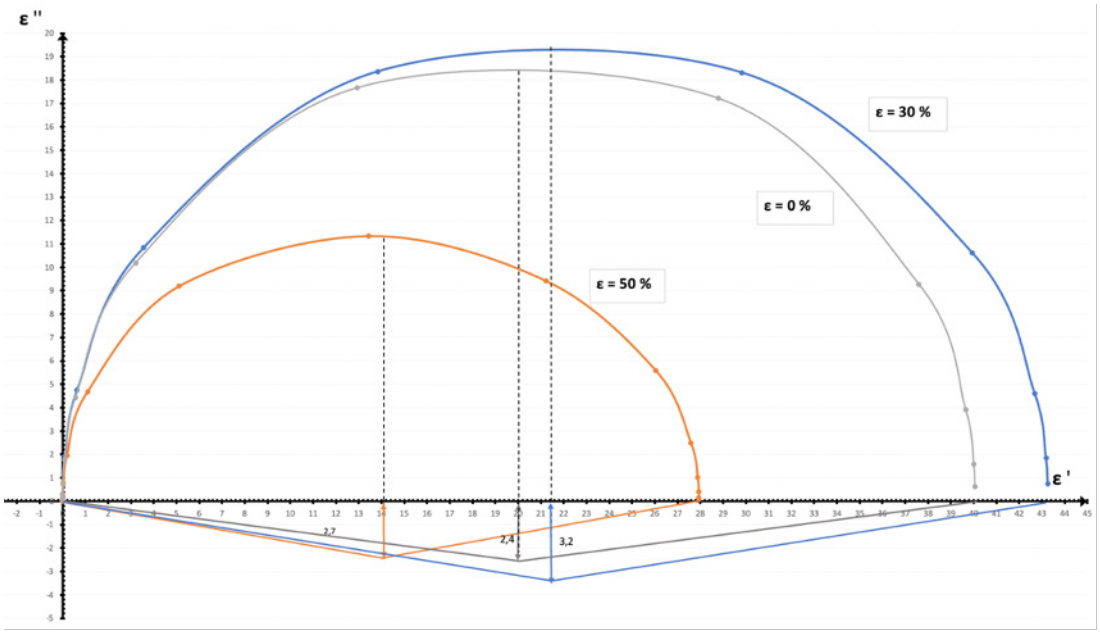

Fig. 6. Dependence of ε' on ε'' for samples with different polymorphic composition and different percentages of pores

Conclusions

The dielectric properties of PVDF polymer films with different structures, polymorphic composition and percentage of pores have been studied. The expediency and relevance of presenting the results of thermal activation spectroscopy in the framework of dielectric spectroscopy at infra-low frequencies is shown. It is revealed that a change in the supramolecular structure entails a shift of the peak of dielectric losses to the low-temperature region.

The peak of dielectric losses for films with different degrees of orientation extraction is shifted to the low temperature region. This is consistent with the results of E_a (Gerasimov et al. 2022), which decrease with an increase in the amount of β-phase.

Interpretation of the results within the framework of the Cole-Cole diagrams indicates a change in the distribution of relaxation times.

Conflict of Interest

The author declares that there is no conflict of interest, either existing or potential.

References

Elyashevich, G. K., Rozova, E. Yu., Karpov, E. A. (1997) *Mikroporistaya polietilenovaya plenka i sposob ee polucheniya [Microporous polyethylene film and method of its production]*. Patent No. RU 2140936 C1. (In Russian)

Gerasimov, D. I., Kuryndin, I. S., Lavrentyev, V. K. et al. (2020) Piezoelectric properties of the oriented porous poly (vynilidene) fluoride films. In: Yu. Gorokhovatsky, D. Temnov, V. Kapralova (eds.). *AIP Conference Proceedings. Vol. 2308. Proceedings of The XV International Conference "Physics of dielectrics" (St. Petersburg, Russia, 5–8 October 2020)*. [S. l.]: AIP Publ., article 030001. [Online]. Available at: https://doi.org/10.1063/5.0033693 (accessed 17.01.2023). (In English)

Gerasimov, D. I., Kuryndin, I. S., Lavrentyev, V. K. et al. (2022) Structure formation and depolarization relaxation in porous polyvinylidene fluoride piezofilms. *Physics of the Solid State*, 64 (10), 300–306. https://link.springer.com/article/10.1134/S1063783422070022 (In English)

Gusev, Yu. A. (2008) *Osnovy dielektricheskoi spektroskopii [Fundamentals of dielectric physics]*. Kazan: Kazan University Publ., 112 p. (In Russian)

Kochervinskii, V. V. (1996) The structure and properties of block poly (vinylidene fluoride) and systems based on it. *Russian Chemical Reviews*, 65 (10), article 865. https://doi.org/10.1070/RC1996v065n10ABEH000328 (In English)

Van Turhour, J. (1975) *Thermally stimulated discharge of polymer electrets*. Amsterdam: Elsevier Publ., 335 p. (In English)

Theoretical physics. Cosmology

UDC 524.8

EDN XBRSNM
https://www.doi.org/10.33910/2687-153X-2023-4-2-59-67

On the temperature of hairy black holes

V. D. Vertogradov ✉[1,2], D. A. Kudryavtsev[1]

[1] Herzen State Pedagogical University of Russia, 48 Moika Emb., Saint Petersburg 191186, Russia
[2] Saint Petersburg Branch of SAO RAS, 65 Pulkovskoe Highway, Saint Petersburg 196140, Russia

Authors

Vitalii D. Vertogradov, ORCID: 0000-0002-5096-7696, e-mail: vdvertogradov@gmail.com

Dmitriy A. Kudryavtsev, e-mail: kudryavtsiev33@gmail.com

For citation: Vertogradov, V. D., Kudryavtsev, D. A. (2023) On the temperature of hairy black holes. *Physics of Complex Systems*, 4 (2), 59–67. https://www.doi.org/10.33910/2687-153X-2023-4-2-59-67 EDN XBRSNM

Received 15 March 2023; reviewed 14 April 2023; accepted 14 April 2023.

Funding: The research was supported by the Russian Science Foundation (Grant No. 22-22-00112).

Abstract. The gravitational decoupling method represents an extremely useful tool to obtain new solutions of the Einstein equations through minimal geometrical deformations. In this paper, we consider a hairy charged black hole obtained by the gravitational decoupling and calculate its Hawking temperature in order to compare it with the case when the hairs are ignored. We have found out that the hair, under some conditions of black hole parameters, affect the Hawking temperature and can increase it. We have also found out that the black hole temperature, in the hairy case, does not depend on the electric charge.

Keywords: hairy black hole, Hawking temperature, charged black hole, gravitational decoupling, Einstein's equations

Introduction

A recent paper (Grib, Pavlov 2022) showed the possibility of phase transition near the event horizon of a black hole. However, the critical Hawking temperature (Hawking 1975) near the horizon at which the phase transition can happen is reached in the vicinity of the event horizonm, while the radius of the region, where this effect is possible, is negligible. When one considers particle collisions, the situation becomes better because the center-of-mass energy can grow unboundly in some processes (Banados et al. 2009; Grib, Pavlov 2015; Vertogradov 2022; Zaslavskii 2012). The region near the event horizon where phase transition can happen is much bigger in comparison to the Hawking temperature (Grib, Pavlov 2022). However, one can try to increase the effect caused by the Hawking temperature by considering the modification of the standard black hole solution and how these modifications affect the black hole temperature.

A well-known theorem in the black hole theory states that a black hole does not have hairs, i. e., it can have only three charges—a mass M, angular momentum j, and electric charge Q. However, it was shown that a black hole can have soft hair (Hawking et al. 2016). Recently, it was understood that one can obtain a hairy black hole by using the gravitational decoupling method (Contreras et al. 2021; Ovalle 2017). In most cases, obtaining new analytical solutions of the Einstein equations is an extremely hard task. One can solve these equations, for example, for the spherical symmetry and the perfect fluid as a source of gravitation. However, if we consider a more realistic case when the perfect fluid is coupled to another matter, it is nearly impossible to obtain the analytical solution. The gravitational decoupling

through minimal geometrical deformation shows the possibility of decoupling two gravitational sources. One can write the energy-momentum tensor as:

$$T_{ik} = \tilde{T}_{ik} + \alpha \Theta_{ik} \ , \tag{1}$$

where $\tilde{T}_{ik}$ is the energy-momentum tensor of the perfect fluid and α is the coupling constant to the energy-momentum tensor Θ_{ik}. It is possible to solve Einstein's field equations for a gravitational source whose energy-momentum tensor is expressed as (1) by solving Einstein's field equations for each component $\tilde{T}_{ik}$ and Θ_{ik} separately. Then, by a straightforward superposition of the two solutions, we obtain the complete solution corresponding to the source T_{ik}. Since the Einstein equations are not linear, this method is effective for the analysis of the solution. It is an especially important tool when one faces the realistic cases, i. e., the stars and collapsing objects whose interior matter is far from the ideal perfect fluid.

By applying this method, a new modification of the Schwarzschild black hole was obtained (Ovalle et al 2018; 2021). These black hole solutions satisfy the strong and dominant energy conditions in the whole region from the event horizon up to infinity. All these solutions have been obtained by small deformations of the Schwarzschild vacuum. The hairy analogy of the Kerr spacetime has been obtained in (Mahapatra, Banerjee 2023). A more realistic case, i. e., the deformation of dynamical background was obtained in (Vertogradov, Misyura 2022).

In this paper, we consider the Hawking temperature for a hairy charged Reissner-Nordstrom black hole obtained by gravitational decoupling through minimal geometrical deformation. We also discuss how it deviates from the black hole when the hairs are ignored. All these models represent a black hole supported by a non-linear electrodynamics.

This paper is organized as follows: in Section 2 we briefly discuss two methods of obtaining the Hawking temperature for a general spherically-symmetric black hole. In Section 3 we explicitly calculate the Hawking temperature for the Reissner-Nordstrom black hole. In Section 4 we consider three models of a hairy black hole and their temperature and compare these results with a no-hair solution. Section 5 provides conclusions and discusses further research. The system of units $c = G = 1$ will be used throughout the paper. Also, we shall adopt the signature − , + , + , +.

Black hole thermodynamics

In this section we review the basic concepts related to the black hole thermodynamics. For more useful and thorough discussion on this subject, see, for example, the review in (Carlip 2009). We consider a spherically-symmetric line element in the form:

$$ds^2 = -fdt^2 + f^{-1}dr^2 + r^2 d\Omega^2 \ , \tag{2}$$

where a lapse function $f = f(r)$ depends upon radial coordinate r, $d\Omega^2 = d\theta^2 + sin^2\,\theta d\phi^2$ is the metric of a unit two-sphere. To describe black holes, it is convenient to write (2) in the form:

$$ds^2 = -\left(1 - \frac{b(r)}{r}\right)dt^2 + \left(1 - \frac{b(r)}{r}\right)^{-1} dr^2 + r^2 d\Omega^2 \quad . \tag{3}$$

Here, we can refer to the function $b(r)$ as the shape function which specifies the shape of the spatial slice. In the limit $\lim\limits_{r \to infty} b(r)$ the shape function can be interpreted as asymptotic mass $2M$. We assume the asymptotic flatness for all models considered in this paper. Metric (3) has horizons at $b(r_h) = r_h$. This equation might have several roots but only the outermost horizon is of the major interest and we will consider only this one. We are interested in the case when $\forall r > r_h \rightarrow b(r) < r$ and $\frac{db(r)}{dr}\Big|_{r=r_h} < 1$. The case $\frac{b(r)}{dr}\Big|_{r=r_h} = 1$ corresponds to an extremal black hole for which the Hawking temperature is zero (Visser 1992). This case will not be considered within this paper. The Hawking temperature is given by:

 https://www.doi.org/10.33910/2687-153X-2023-4-2-59-67

$$k_b T_h = \frac{\hbar \varkappa}{2\pi} , \tag{4}$$

where k_b is the Boltzmann constant, T_h is the Hawking temperature and $\varkappa$ is the surface gravity which, for metric (2), has the form:

$$\varkappa = \lim_{r \to r_h} \frac{1}{2} \frac{df}{dr} . \tag{5}$$

Substituting a lapse function in form (3), one obtains:

$$\varkappa = \frac{1}{2r_h} \left[1 - b'(r_h) \right] , \tag{6}$$

where a dash corresponds to the derivative with respect to the radial coordinate r.

Another way to obtain the Hawking temperature is to use Euclidean signature techniques. By the formal transformation to the imaginary time $t \to it$, we get:

$$ds^2 = f dt^2 + f^{-1} dr^2 + r^2 d\Omega^2 . \tag{7}$$

Again, we are interested in the outermost horizon at $r = r_h$ and discard the whole $r < r_h$ region. Furthermore, we assume the lapse function f in the form given by (3) and also demand that a black hole is not an extremal one. Taylor expand near the horizon gives:

$$1 - \frac{b(r)}{r} \approx \left[1 - b'(r_h) \right] \frac{r - r_h}{r_h} . \tag{8}$$

Substituting (8) into (7), one obtains:

$$ds^2 \approx \frac{\left(1 - b'(r_h)\right)(r - r_h)}{r_h} dt^2 + \left[\frac{\left(1 - b'(r_h)\right)(r - r_h)}{r_h} \right]^{-1} dr^2 + r_h^2 d\Omega^2 . \tag{9}$$

By introducing a new variable R:

$$dR = \left[\frac{\left(1 - b'(r_h)\right)(r - r_h)}{r_h} \right]^{-\frac{1}{2}} dr , \tag{10}$$

one can transform metric (9) to obtain:

$$ds^2 \approx \frac{\left[1 - b'(r_h) \right]^2}{4r_h^2} R^2 dt^2 + dR^2 + r_h^2 d\Omega^2 . \tag{11}$$

The (t, R) part of this metric is similar to a flat two-plane in polar coordinates, with imaginary time t serving as the angular coordinate. In order to avoid a conical singularity, one should demand that $\frac{1 - b'(r_h)}{2r_h} t$ has a period 2π, i. e., t has a period β which is given by:

$$\beta = \frac{4\pi r_h}{1 - b'(r_h)} . \tag{12}$$

According to (Gibbons, Hawking 1977), this imaginary time t is interpreted as the existence of the thermal bath of a temperature $k_b T_h = \frac{\hbar}{\beta}$, which explicitly gives:

$$k_b T_h = \frac{\hbar}{4\pi r_h}\left(1 - b'\left(r_h\right)\right), \tag{13}$$

which coincides with (4).

The Hawking temperature of the Reissner-Nordstrom black hole

In this section we will apply the method described in the previous section to the Reissner-Nordstrom solution which describes a charged static black hole. The result of this section is well-known and can be found, for example, in (Brown et al. 1994; Poisson 2007; Visser 1992). We rederive these results only in order to compare them with hairy black holes.

Here and in what follows, we will use the system of units $k_b = \hbar = 1$. The lapse function f (2) in the Reissner-Nordstrom case is given by:

$$f\left(r\right) = 1 - \frac{2m}{r} + \frac{Q^2}{r^2}. \tag{14}$$

The shape function $b\,(r)$ (3) and its derivative are given by:

$$b\left(r\right) = 2M - \frac{Q^2}{r}, \qquad b'\left(r\right) = \frac{Q^2}{r^2}. \tag{15}$$

The Reissner-Nordstrom black hole has two horizons which are located at:

$$r_{\pm} = M \pm \sqrt{M^2 - Q^2}. \tag{16}$$

Here, as we stated above, we are interested only in the outermost horizon, so that $r_h = r_+$. The cases $Q^2 > M^2$ and $Q^2 = M^2$, which correspond to a naked singularity and an extremal Reissner-Nordstrom black hole, will not be considered in this paper.

The surface gravity $\varkappa$ at the horizon is given by:

$$\varkappa = \frac{1}{r_h}\left(1 - \frac{Q^2}{r_h^2}\right). \tag{17}$$

And the Hawking temperature is:

$$T_h = \frac{1}{4\pi r_h}\left(1 - \frac{Q^2}{r_h^2}\right). \tag{18}$$

Note, that in the extremal case $M^2 = Q^2$, the horizon is located at $r_h = M$, which gives $1 - \frac{Q^2}{r_h^2} = 0 \to T_h = 0$.

Thermodynamics of hairy black holes

Using the gravitational decoupling method, a recent paper (Ovalle et al. 2021) introduced a new solution which describes the exterior geometry of hairy black holes. In this section, we will calculate the Hawking temperature and compare the results with a usual Reissner-Nordstrom black hole in order to find out how primary hairs affect the Hawking temperature.

Model 1

This model can be interpreted as a black hole supported by a non-linear electrodynamics. The other two models can be obtained from this model by defining the electric charge Q as a function of the Schwarzschild mass M and primary hairs α and $l_0 = \alpha l$.

The lapse function f for Model 1 is given by:

$$f\left(r\right) = 1 - \frac{2\mu}{r} + \frac{Q^2}{r^2} - \frac{\alpha\left(\mu - l_0/2\right)e^{-r/\left(\mu - l_0/2\right)}}{r}. \tag{19}$$

Here, $\mu = M + l_0/2$, M is the Schwarzschild mass, α is the coupling constant and $l_0 = \alpha l$ is the primary hair, Q can be interpreted as the electric charge of a black hole. The influence of the geodesic

 https://www.doi.org/10.33910/2687-153X-2023-4-2-59-67

motion of primary hairs was studied in (Ramos et al. 2021). The influence of these parameters for the thermodynamics properties in a hairy Schwarzschild black hole was investigated in (Cavalcanti et al. 2022). The shadow properties of hairy black hole are covered in (Vagnozzi et al. 2022). The Schwarzschild solution is the limit of $\alpha \to 0$.

The event horizon equation is given by $f(r_h) = 0$, which can be solved with respect to l_0 to give:

$$l_0 = r_H - 2M + \frac{Q^2}{r_H} - \alpha M e^{-r_H/M} \ . \tag{20}$$

We have several restrictions on the parameters. First of all, one should realize that like in the pure Reissner-Nordstrom case, one should impose certain conditions on the parameters in order to avoid a naked singularity in the usual Reissner-Nordstrom case. They include M and charge Q - $M^2 \geq Q^2$. However, the condition $M^2 = Q^2$ is not forbidden because in this case the hairy black hole (19) is not an extremal one. Also, this model satisfies the dominant energy condition only when $r \geq 2M$, so we do not consider the region $0 \leq r \leq 2M$ and demand $r_h \geq 2M$ to satisfy the energy condition. The fulfilling of the dominant energy condition also imposes the following restrictions on the parameters Q and l:

$$|Q| \geq \alpha \frac{M^2}{e^2} \ , \qquad l \geq \frac{M}{e^2} \ . \tag{21}$$

The Hawking temperature (4) $T_h = \frac{\varkappa}{4\pi}$ is given in terms of the surface gravity $\varkappa$ which for this model reads:

$$2\varkappa = 1 + \frac{2M}{r_h^2} - \frac{2Q^2}{r_h^3} + \frac{\alpha r_h e^{-r_h/(M-l_0/2)} + \alpha\left(M - l_0/2\right)e^{-r_h/(M-l_0/2)}}{r_h^2} \ . \tag{22}$$

So the Hawking temperature is:

$$T_h = \frac{1}{4\pi} 1 + \frac{2M}{r_h^2} - \frac{2Q^2}{r_h^3} + \frac{\alpha r_h e^{-r_h/(M-l_0/2)} + \alpha\left(M - l_0/2\right)e^{-r_h/(M-l_0/2)}}{r_h^2} \ . \tag{23}$$

Fig.1 is plotted for $M = 1$, $\alpha = 0.5$, $Q = 0.9$. This figure shows the dependence of the primary hair l_0 on the horizon location (a blue curve). The horizontal red line corresponds to $l_0 = \alpha \frac{M}{e^2}$. We see that at $r_h \geq 2.061$ the dominant energy condition is always held.

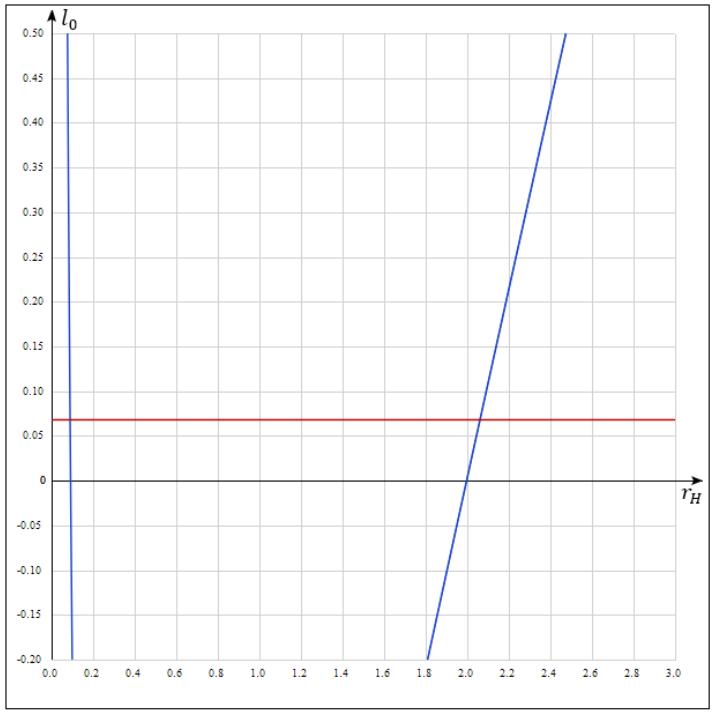

Fig. 1. The event horizon function

Fig. 2 shows the dependence of the Hawking temperature T_h on the horizon location. Three horizontal lines correspond to the Hawking temperature of a usual Reissner-Nordstrom black hole. We have picked up the following parameters for horizontal lines: $M = 1$, $Q = 0.5$ (a red line); $Q = 0.9$ (a green line) and $Q = 0.99$ (an orange line). In this model, the Hawking temperature of a hairy black hole does not depend on the electric charge Q and is the function only of mass M, coupling constant $\alpha = 0.5$ and horizon location r_h, i. e., $T_h \equiv T_h(M, \alpha, r_h)$ (the corresponding curve is blue). We can easily see that at $r_h \in (2.061, 0.212)$ for $Q = 0.$; $r_h \in (2.061, 2.481)$ $r_h \in (2.061, 2.481)$ for $Q = 0.9$ and $r_h \in (2.061, 4.583)$ for $Q = 0.99$, the Hawking temperature is higher than for a usual Reissner-Nordstrom black hole. It means that in these cases the phase transition, which can happen near the event horizon, can be fairer than in a no-hair black hole. One can also see that when one considers an extremal Reissner-Nordstrom black hole, then the Hawking temperature is absent but in the hairy case it is not zero. So, we can conclude that for the first model the primary hairs can increase the Hawking temperature in comparison with the usual Reissner-Nordstrom case.

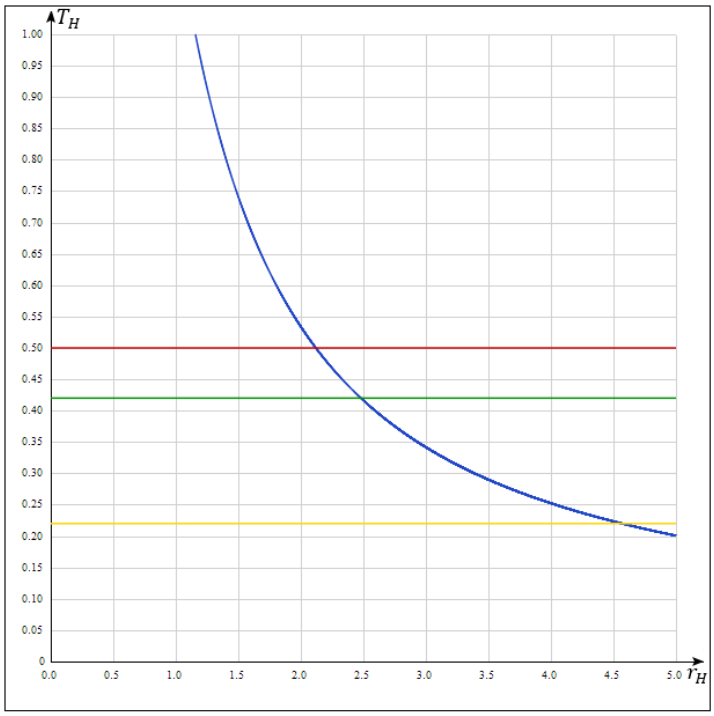

Fig. 2. The Hawking temperature. Model 1

Model 2

As we stated in the previous subsection, the ensuing models differ from the first one by the appropriate choice of the function Q. In this model Q is given by:

$$Q^2 = L_0 M \left(2 + \alpha e^{-l_0/M}\right). \tag{24}$$

Substituting this into (19), one obtains:

$$f = 1 - \frac{2M + l_0}{r} + \frac{2l_0 M}{r^2} - \frac{\alpha M e^{-r/M}}{r^2}\left(r - l_0 e^{\frac{r-l_0}{M}}\right). \tag{25}$$

For this choice of the charge function the horizon equation is:

$$r_h = l_0 \ . \tag{26}$$

Like in the previous subsection, the Hawking temperature is given in terms of the first derivative of the lapse function f', which in this case reads:

 https://www.doi.org/10.33910/2687-153X-2023-4-2-59-67

$$f' = \frac{2M + l_0}{r_h^2} - \frac{4l_0 M}{r_h^3} + \frac{\alpha e^{-r_h/M}\left(r_h - 2M\right)}{r_h^3}\left(r_h - l_0 e^{\frac{r_h - l_0}{M}}\right) + \\ + \frac{\alpha M e^{-r_h/M}}{r_h^2}\left(\frac{l_0}{M} e^{\frac{r_h - l_0}{M}} - 1\right). \tag{27}$$

In this model, the dominant energy condition is always held for $r \geq 2$. Again, like in the first model, the Hawking temperature, after substituting l_0, does not depend on the electric charge of a hairy black hole.

Fig. 3 shows how the Hawking temperature T_H depends on the event horizon location r_h. The choice of the parameters is like in the first model. Fig. 3 differs from Fig. 2 only by the blue curve, which corresponds to the Hawking temperature of a hairy black hole. From the figure, one can see that the temperature of a hairy black hole is always less than in a no-hair case. The only exception is an extremal Reissner-Nordstrom black hole. So we can conclude that one can consider a bigger region where phase transition can happen only for an extremal Reissner-Nordstrom black hole. In other cases, the region is smaller than in a no-hair case.

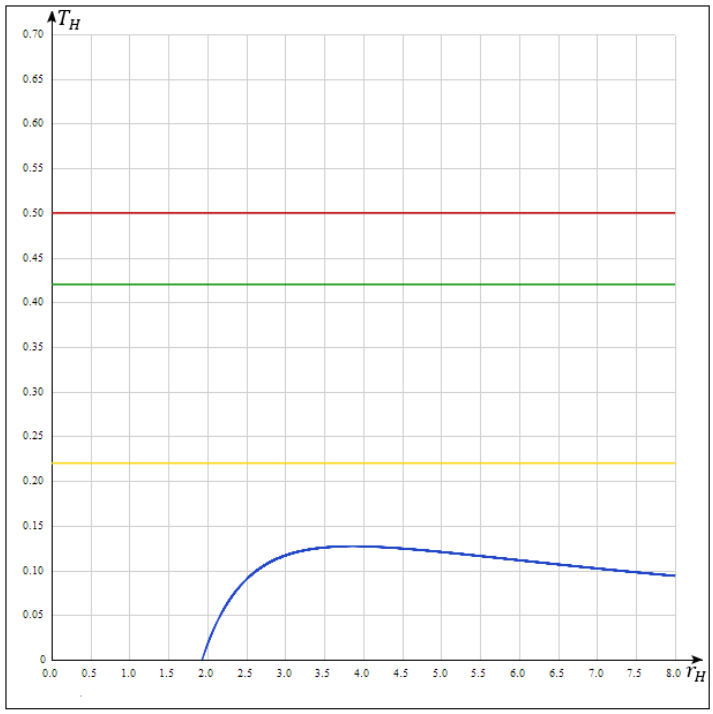

Fig. 3. The Hawking temperature. Model 2

Model 3

For the last model, which we consider within this paper, the charge function is given by:

$$Q^2 = \alpha M\left(2M + l_0\right)e^{-\frac{2M + l_0}{M}}. \tag{28}$$

Its substitution into the lapse function f (19), gives us:

$$f = 1 - \frac{2M + l_0}{r} - \frac{\alpha M}{r^2} e^{-r/M}\left(r - \left(2M + l_0\right)e^{\frac{r - 2M - l_0}{M}}\right). \tag{29}$$

The horizon in this model is located at:

$$r_H = 2M + l_0\ . \tag{30}$$

The first derivative of the lapse function, which gives the main contribution to the Hawking temperature, reads:

$$f' = \frac{2M + l_0}{r_h^2} + \frac{2\alpha M}{r_h^3} e^{-r_h/M} \left(r_h - (2M + l_0) e^{\frac{r_h - 2M - l_0}{M}} \right) + \\ + \frac{\alpha}{r_h^2} e^{-\frac{r_h}{M}} (r_h - 2M + l_0) e^{\frac{r_h - 2M - l_0}{M}} - \frac{\alpha M}{r_h^2} e^{-\frac{r_h}{M}} \left(1 - (2 + l_0 / M) e^{\frac{r_h - 2M + l_0}{M}} \right) . \quad (31)$$

In this model, the dominant energy condition is held when $r_h > 2.067$. It should not be a surprise that for this model the Hawking temperature does not depend on the electric charge of a hairy black hole again.

Fig. 4 is plotted for the same parameters as in the two previous cases and shows the Hawking temperature T_H as the function of the event horizon location r_h. From the figure, one can see that the hairy black hole temperature at $r_h \in$ (2.067, 2.074 for Q = 0.5; $r_h \in$ (2.067, 2.444) for Q = 0.9 and $r_h \in$ (2.067, 4.583) for Q = 0.99, respectively, is bigger than in a no-hair Reissner-Nordstrom black hole. This model shows that under the proper choice of parameters, the region where the phase transition can take place is bigger than in a usual charged black hole.

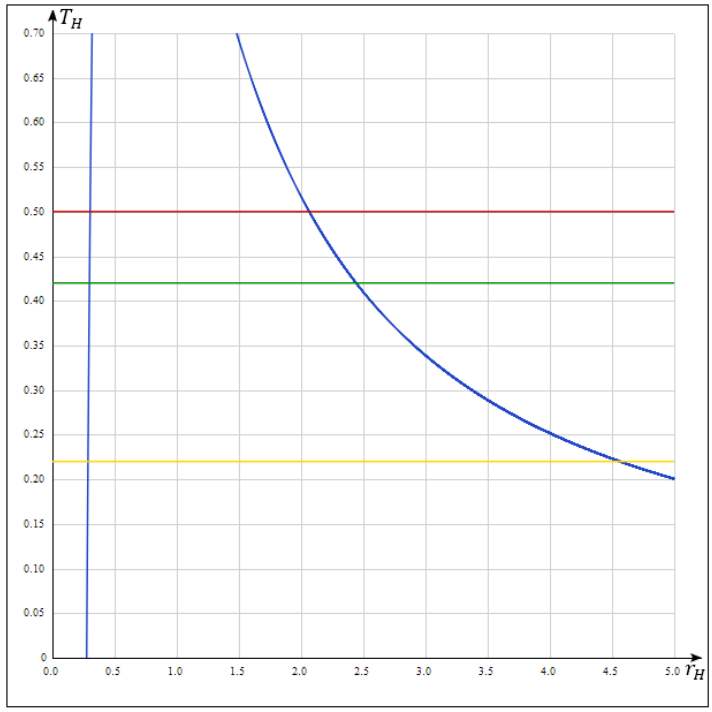

Fig. 4. The Hawking temperature. Model 3

Conclusions

In this paper, we have derived the Hawking temperature of the hairy charged black holes by gravitational decoupling. These black holes can be interpreted as ones supported by a non-linear electrodynamics. The main analytical result obtained within this paper is that the Hawking temperature does not depend on the electric charge Q of a hairy black hole.

We have considered three models and showed that the Hawking temperature is not zero in the case of an extremal no-hair Reissner-Nordstrom black hole. However, in the second model, the Hawking temperature of the hairy charged black hole is always less than one in the case of a non-extremal no-hair charged black hole. For the first and third models, we showed that under a certain choice of primary hairs, one can obtain the black hole temperature higher than in a non-extremal no-hair Reissner-Nordstrom

 https://www.doi.org/10.33910/2687-153X-2023-4-2-59-67

black hole. It means that the region, where the phase transition can take place in the first and the third models, is bigger than the one in a usual charged black hole.

Further research will focus on the entropy, heat capacity and stability of the hairy black hole. It will also identify the exact value of r at which the phase transition can take place. Besides, our follow-up papers will investigate particle collisions, corresponding temperature and how hairs of a black hole affect collision.

Conflict of Interest

The authors declare that there is no conflict of interest, either existing or potential.

Authors contribution

The authors have made an equal contribution to the preparation of the paper.

References

Banados, M., Silk, J., West, S. M. (2009) Kerr black holes as particle accelerators to arbitrarily high energy. *Physical Review Letters*, 103 (11), article 111102. https://doi.org/10.1103/PhysRevLett.103.111102 (In English)

Brown, J. D., Creighton, J., Mann, R. B. (1994) Temperature, energy, and heat capacity of asymptotically anti–de Sitter black holes. *Physical Review D*, 50 (10), article 6394. https://doi.org/10.1103/PhysRevD.50.6394 (In English)

Carlip, S. (2009) Black hole thermodynamics and statistical mechanics. *Lecture Notes in Physics*, 769, 89–123. https://doi.org/10.1007/978-3-540-88460-6_3 (In English)

Cavalcanti, R. T., Alves, K. D. S., Hoff da Silva, J. M. (2022). Near-horizon thermodynamics of hairy black holes from gravitational decoupling. *Universe*, 8 (7), article 363. https://doi.org/10.3390/universe8070363 (In English)

Contreras, E., Ovalle, J., Casadio, R. (2021) Gravitational decoupling for axially symmetric systems and rotating black holes. *Physical Review D*, 103 (4), article 044020. https://doi.org/10.1103/PhysRevD.103.044020 (In English)

Gibbons, G. W., Hawking, S. W. (1977) Action integrals and partition functions in quantum gravity. *Physical Review D*, 15 (10), article 2752. https://doi.org/10.1103/PhysRevD.15.2752 (In English)

Grib, A. A., Pavlov, Yu. V. (2015) Are black holes totally black? *Gravitation and Cosmology*, 21 (1), 13–18. https://doi.org/10.1134/S0202289315010065 (In English)

Grib, A. A., Pavlov, Yu. V. (2022) On phase transitions near black holes. *JETP Letters*, 116 (8), 493–499. https://doi.org/10.1134/S0021364022601907 (In English)

Hawking, S. W. (1975) Particle creation by black holes. *Communications in Mathematical Physics*, 43 (3), 199–220. https://doi.org/10.1007/BF02345020 (In English)

Hawking, S. W., Perry, M. J., Strominger, A. (2016) Soft hair on black holes. *Physical Review Letters*, 116 (23), article 231301. https://doi.org/10.1103/PhysRevLett.116.231301 (In English)

Mahapatra, S., Banerjee, I. (2023) Rotating hairy black holes and thermodynamics from gravitational decoupling. *Physics of the Dark Universe*, 39, article 101172. https://doi.org/10.1016/j.dark.2023.101172 (In English)

Ovalle, J. (2017) Decoupling gravitational sources in general relativity: From perfect to anisotropic fluids. *Physical Review D*, 95 (10), article 104019. https://doi.org/10.1103/PhysRevD.95.104019 (In English)

Ovalle, J., Casadio, R., Contreras, E., Sotomayor, A. (2021) Hairy black holes by gravitational decoupling. *Physics of the Dark Universe*, 31, article 100744. https://doi.org/10.1016/j.dark.2020.100744 (In English)

Ovalle, J., Casadio, R., da Rocha, R. et al. (2018) Black holes by gravitational decoupling. *The European Physical Journal C*, 78, article 960. https://doi.org/10.1140/epjc/s10052-018-6450-4 (In English)

Poisson, E. (2007) *A relativist's toolkit: The mathematics of black-hole mechanics*. Cammbridge: Cambridge University Publ., 233 p. (In English)

Ramos, A., Arias, C., Avalos, R., Contreras, E. (2021) Geodesic motion around hairy black holes. *Annals of Physics*, 431, article 168557. https://doi.org/10.1016/j.aop.2021.168557 (In English)

Vagnozzi, S., Rittick, R., Yu-Dai, T. et al. (2022) Horizon-scale tests of gravity theories and fundamental physics from the Event Horizon Telescope image of Sagittarius A*. *arXiv*, article 2205.07787. [Online]. Available at: https://doi.org/10.48550/arXiv.2205.07787 (accessed 10.03.2023). (In English)

Vertogradov, V. (2022). On the particle collisions during gravitational collapse of Vaidya spacetimes. *arXiv:2211.16189*. [Online]. Available at: https://doi.org/10.48550/arXiv.2211.16189 (accessed 17.01.2023). (In English)

Vertogradov, V., Misyura, M. (2022) Vaidya and generalized vaidya solutions by gravitational decoupling. *Universe*, 8 (11), article 567. https://doi.org/10.3390/universe8110567 (In English)

Visser, M. (1992) Dirty black holes: Thermodynamics and horizon structure. *Physical Review D*, 46 (6), article 2445. https://doi.org/10.1103/PhysRevD.46.2445 (In English)

Zaslavskii, O. B. (2012) Acceleration of particles by black holes as a result of deceleration: Ultimate manifestation of kinematic nature of BSW effect. *Physics Letters B*, 712 (3), 161–164. https://doi.org/10.1016/j.physletb.2012.05.009 (In English)

Physics of Semiconductors. Physics of thin films

UDC 538.935

EDN TDFUBE
https://www.doi.org/10.33910/2687-153X-2023-4-2-68-74

Electric transport in thin modified films of selenide and sulfide of arsenic

V. T. Avanesyan✉[1]

[1] Herzen State Pedagogical University of Russia, 48 Moika Emb., Saint Petersburg 191186, Russia

Author

Vachagan T. Avanesyan, ORCID: 0000-0001-5772-8375, e-mail: avanesyan@mail.ru

For citation: Avanesyan, V. T. (2023) Electric transport in thin modified films of selenide and sulfide of arsenic. *Physics of Complex Systems*, 4 (2), 68–74. https://www.doi.org/10.33910/2687-153X-2023-4-2-68-74 EDN TDFUBE

Received 4 March 2023; reviewed 31 March 2023; accepted 31 March 2023.

Funding: The study did not receive any external funding.

Abstract. In the studied ChGS the effect of modification influence on the nature of the temperature dependence of conductivity was found. The value of the latter increases with a decrease in the band gap and, accordingly, with an increase of the activation energy. This energy correlates with the change in the height of the potential barrier at the contact between the metal and the chalcogenide glassy semiconductor for different compositions of As_2Se_3 and As_2S_3 materials. The significant role of a single pair of electrons belonging to the atoms of the modifying impurity is noted. The pair of electrons is responsible for the realization of disordered and defective structure and for the formation of the energy system of local states that affect the process of charge carrier transfer.

Keywords: modification, conductivity, activation energy, chalcogenide glassy semiconductor, single pair of electrons

Introduction

An analysis of scientific and technical literature shows that chalcogenide glassy semiconductors are promising materials for use in various fields of science and technology (Chirita, Prilepov 2022). Binary compounds As_2X_3 (X = S, Se) have optical, electrical, and mechanical properties that allow these materials to be used in modern technology, in particular, in telecommunications, medicine, and instrumentation. Amorphous chalcogenide materials are of great interest due to their exceptional structural, electronic and optical properties. Obtaining and studying films based on chalcogenide semiconductors, such as As-Se and As-S, remains an urgent task both from the fundamental and from the applied point of view. Due to this, chalcogenide glassy semiconductors (ChGS) are used in photonics, optoelectronics, micro- and nanoelectronics as devices with optical and electrical memory, media for recording and storing optical and holographic information, in integrated optics, as light guides, etc. (Mehta 2006). ChGS have a number of unique properties that are either partially present or completely absent in crystalline semiconductors: reversible electrical switching and memory effect, photoinduced structural transformations, etc. Also, the advantages of chalcogenide glassy semiconductors include high resistance, a wide glass transition region, and high resistance to moisture. Variation in the composition of ChGS makes it possible to control their properties (optical, thermal, and mechanical). It is known that the structure of ChGS based on arsenic contains structural units such as AsSe, AsS, with homopolar bonds As-As, S-S, Se-Se and heteropolar As-Se, As- S.

Despite the numerous literature data on the study of the structural features, electrical and optical properties of amorphous As_2X_3 (X = Se, S) films, the issues related to the features of the methods for

obtaining amorphous thin films and their influence on the characteristics of the studied films remain unclear (Nguyen et al. 2018). The introduction of metal impurities into the basic grid of the material under study leads to the rearrangement of some chemical bonds and, thus, the appearance of defects, which improves some parameters of the substance. This work presents the results of the study on the influence of the modifier (Pb) on the electrical conductivity of binary compounds of As_2Se_3 and As_2Se_3 ChGS.

Experimental methods

We used the method of formation of ChGS films in vacuum. In this method, thermal deposition, deposition of films in a quasi-closed volume made it possible to achieve the closest approximation to the stoichiometric composition in the vapor phase. The deposition was usually carried out on glass substrates located at a distance of 10–30 cm from the evaporator, depending on the composition of the evaporated material. The substrates were not subjected to forced heating or cooling.

The film was deposited at a rate of 0.1…0.5 μm/min. using conventional thermal evaporation. The thickness of the obtained films was measured using an interferometer and varied within 0.5…5 μm. The conductivity of the modified chalcogenide glass samples at direct current was determined by the leakage current from the time dependence of the absorption current. Immediately before the measurement cycle, the sample was annealed in a cryostat for one hour at T= 420 K.

Results and discussion

Small deviations in the local structure of glass atoms and breaking of chemical bonds can lead to the formation of local (fluctuation) levels in the band gap of a glassy semiconductor, the concentration of which is described by the following formula (Gubanov 1963):

$$N = N_o \frac{4\varepsilon\sqrt{Z}}{2\sqrt{2\pi}} \exp\left(-\frac{2}{\varepsilon^2 Z^2 \varphi^2}\right),$$

where N_o is the number of valence bonds in 1 cm^3, Z is the number of valence bonds in the first coordinate sphere, e is the degree of short-range order violation, ϕ is the coefficient that takes into account the degree to which the wave functions of neighboring atoms overlap.

According to the available measurements of currents limited by the space charge (Zhang, Pantelides 2012), short-range order fluctuations of ChGS (As_2Se_3) create localized levels in the middle of the band gap with a density of 10^{16} cm^{-3} eV^{-1}. The weak effect of impurities on the ChGS conductivity, which is characteristic of arsenic ChGS, was explained according to the ideas of Gubanov–Mott (Kolomiets et al. 1982) by the fact that the glass structure can rearrange around impurity atoms, saturating all chemical bonds. Previously (Kolomiets et al. 1982), it was shown that impurity can effectively affect the electrical properties of ChGS during cold alloying, at which the temperature should not exceed the softening temperature of an amorphous substance. An important point in this case is the choice of the dopant, since in this method of doping the impurity atoms have a much lower possibility for incorporation into the glass atomic framework with the fulfillment of the necessary valence conditions.

Modification of ChGS, i. e., doping with high doses of impurity of a number of transition metals, leads to a sharp increase in conductivity with a relatively slight change in the optical properties of these materials. In this case, an impurity band with the ionization energy depending on the concentration and the type of the modifier is formed in the ChGS band gap (Ghayebloo et al. 2017). The formation of cross-links between molecular chains due to the presence of modifier atoms can lead to an expansion of the band of localized states of the valence band and a corresponding decrease in the band gap. As follows from the experimental data presented in Fig.1 and Fig. 2, temperature dependences of specific conductivity σ of samples As_2Se_3<Pb> and As_2S_3 <Pb> have the form characteristic of most ChGSs and are satisfactorily described by the Arrhenius law (Moynihan et al. 1982):

$$\sigma = \sigma_o \exp\left(-\frac{E_A}{kT}\right),$$

where the pre-exponential factor σ_o is a constant that depends on the properties of the material and is characterized by a single value of the activation energy E_A, T is the absolute temperature.

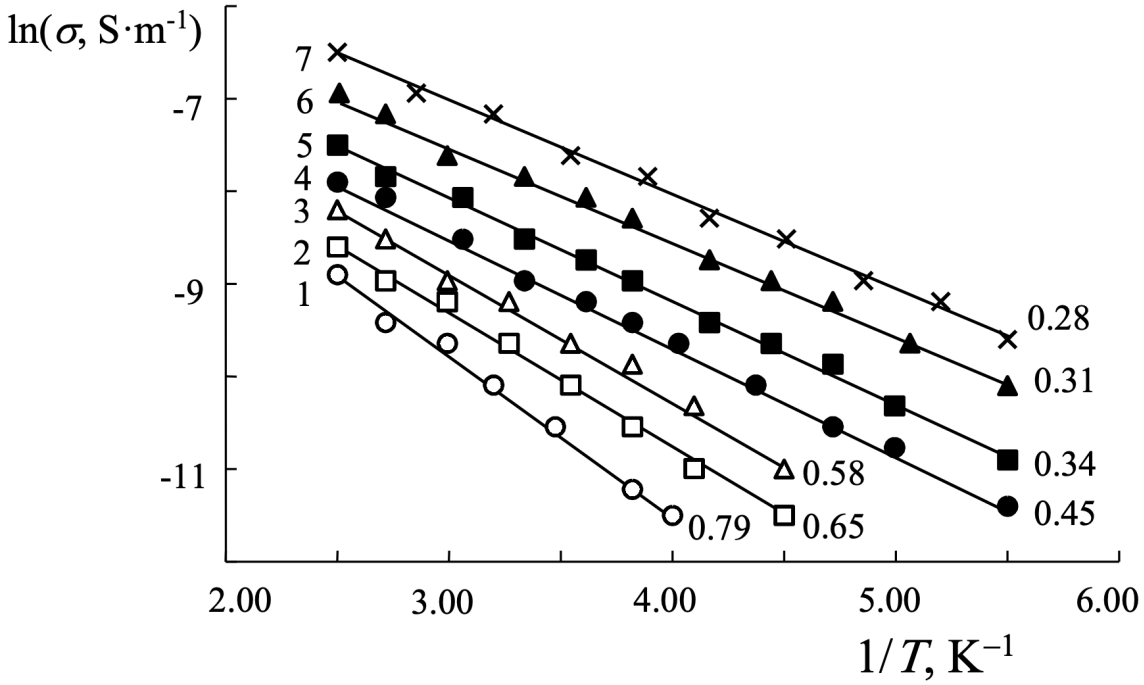

Fig. 1. Temperature dependence of the conductivity of As2Se3 films at different modifier contents:
1—undoped ChGS, 2—1.5, 3—3.2, 4—4.1, 5—6.4, 6—8.3, 7—10.5 at. % Pb.
The values of the activation energy on the dependences are given in eV

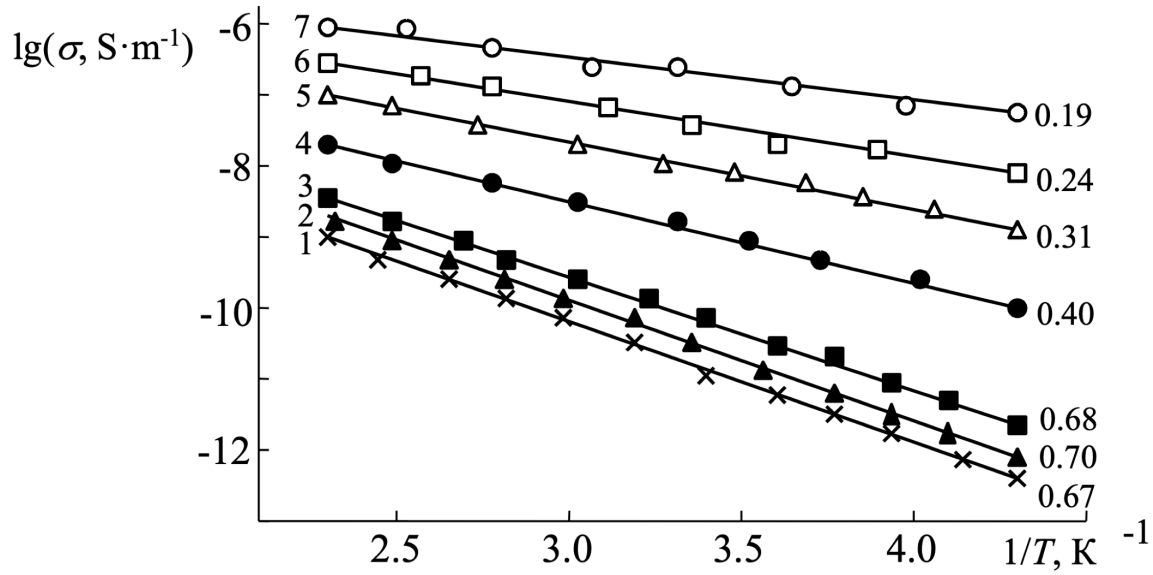

Fig. 2. Temperature dependence of the conductivity of As_2S_3 films at different modifier contents:
1—undoped ChGS, 2—1.3, 3—3.0, 4—4.3, 5—6.2, 6—8.1, 7—9.5 at. % Pb.
The values of the activation energy on the dependences are given in eV

For the modified ChGS films, a larger value of the conductivity increment $\Delta\sigma$ was observed compared to the ChGS of the initial composition. Fig. 3 shows the dependences of the activation energy of the studied samples on the content of the modifying impurity. It follows from the analysis of the obtained results that the parameter σ corresponds to an exponential dependence with a sharply decreasing

 https://www.doi.org/10.33910/2687-153X-2023-4-2-68-74

activation energy at small amounts of the introduced modifier from 0.32 to 0.15 eV and a slow decrease in the value of the latter with a further increase in the percentage of the modifier. The observed decrease in the band gap E_g with the introduction of a modifier is apparently due to the fact that some of the Pb atoms embedding in the glass network saturate all their valence bonds and, thereby, form new compounds of the solid solution type. In this case, the parameter E_g is a certain average value between the band gap of arsenic selenide and the band gap of lead selenide, which is a narrower gap semiconductor (Chu, Sher 2007).

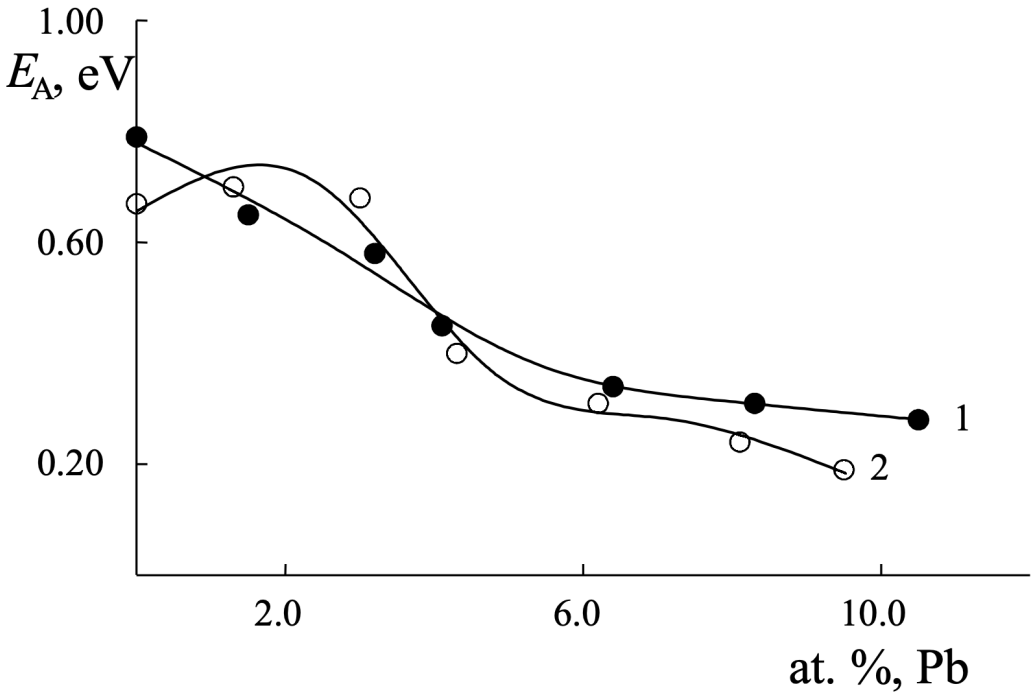

Fig. 3. Dependence of the activation energy of film conductivity As2Se3 (1) and As2S3 (2) on the impurity content

As the results of the experiments performed in the As-Se and As-S systems show, E_A changes little with composition variation but is greater in value for a material with excess sulfur content and less arsenic content with an increase in the amount of selenium. Thus, we can conclude that direct current conductivity is more sensitive to changes in the constant σ_o. At alternating current, both systems retain the dependence of conductivity on composition. Compounds that are close to stoichiometric have a larger E_A value for the As-Se system and a smaller one for As-S. Since there are no pronounced features on the electrical conductivity curves in the studied temperature range, it can be assumed that the Fermi level remains near the middle of the band gap, and the manifestation of the dominant type of conductivity with an increase in the Pb content is due to a change in the ratio of the hole and electron mobilities. We noted the presence of the maximum and minimum values of the parameters σ and E_A depending on the compositional composition of the studied samples, and the introduction of a small percentage (1 ... 1.5%). In the processes of switching and breakdown of ChGS, the field dependence of electrical conductivity plays a decisive role. It follows from the results of numerous previous measurements that ChGSs—in particular, As_2Se_3 and As_2S_3—are quite high-resistant and can be used under conditions of a sufficiently high electric field strength. In the present study, an exponential dependence of the conductivity on the applied field was observed (Figs. 4, 5), which can be interpreted assuming the existence of a current limited by the space charge of a uniform distribution of local states per unit volume in the region of the Fermi level (Zhang, Pantelides 2012).

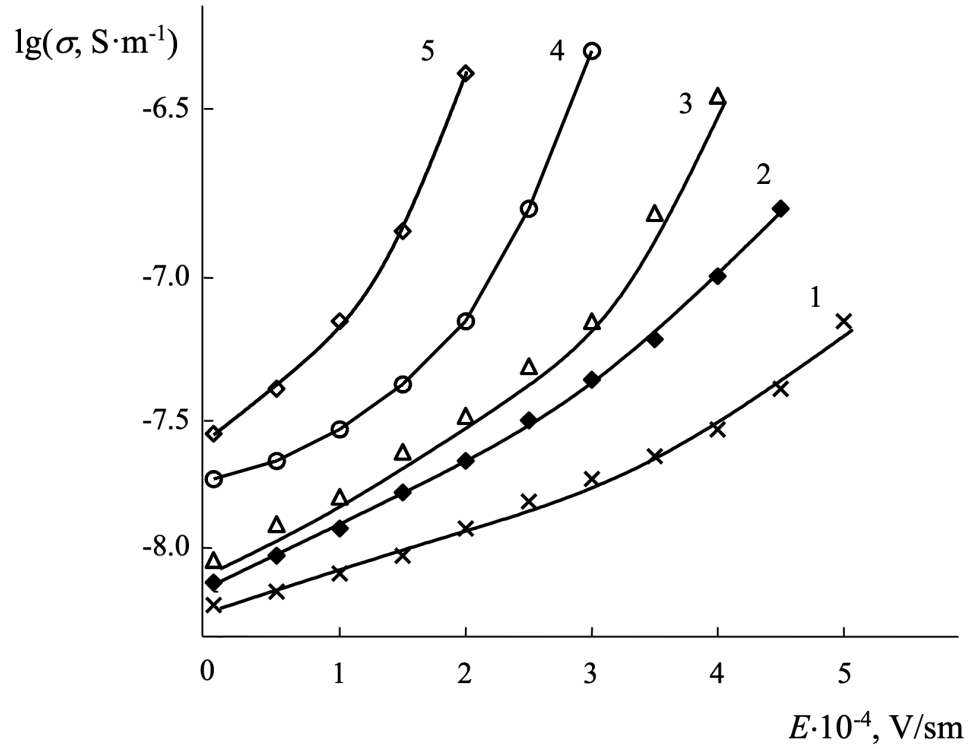

Fig. 4. Field dependence of As_2Se_3 films with different modifier contents: 1—undoped ChGS, 2—1.5, 3—3.2, 4—4.1, 5—6.4 at. % Pb

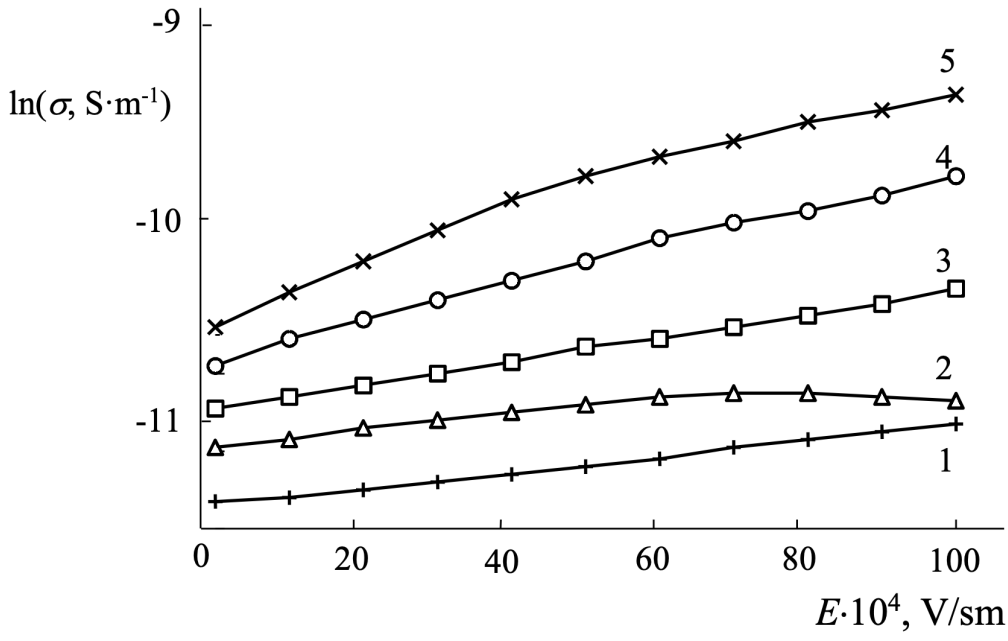

Fig. 5. Field dependence of As_2S_3 films with different contents of the modifier (Pb): 1—undoped ChGS, 2—1.3, 3—3.0, 4—4.3, 5—6.2 at. % Pb

A change in the thickness of the samples has an insignificant effect on the nature of the change in the function $\sigma(E)$ under conditions of constant temperature. Starting from a certain value of the electric field strength ($E_1 < 3 \times 10^{-4}$ V/cm), the obtained characteristics are satisfactorily rectified, answering for most

 https://www.doi.org/10.33910/2687-153X-2023-4-2-68-74

samples the dependence $\sigma = \sigma_o \exp(E/E_o)$. With an increase in the electric field strength in the region of $E > 3 \times 10^{-4}$ V/cm, the values of σ increase.

One of the main mechanisms interpreting the nonohmic conductivity in ChGSs (Nardone et al. 2012) assumed that the mobility of localized states depends on the electric field during the transfer of thermally activated charge carriers over multiple barriers.

According to Kazakova and Lebedev, the introduction of a modifier enhances recombination rather than generation processes (Kazakova, Lebedev 1998). Taking into account that holes remain the dominant type of charge carriers, we can assume that the Fermi level E_F shifts to the valence band. This may be due to the fact that some of the modifier atoms form acceptor-type impurity centers. Such a shift in E_F leads to an increase in conductivity and photoconductivity. In ChGS with a high content of Se compared to the stoichiometric composition, the modifier can form a compound (PbSe) without breaking the As-Se bonds. The modifier in this case becomes more stable and less mobile. The formation of the same compound in an As-enriched composition can lead to multiple breaking of the corresponding bonds with the formation of an excessive number of As atoms in the defect structure. Electrically active centers in the band gap of an amorphous semiconductor can be created by atoms of elements that, in addition to orbitals capable of forming strong covalent bonds, also have a set of other orbitals capable of interacting with the orbitals of the surrounding atoms. With a change in the composition of CGS glass, the formation of additional As–As structural bonds, which determine the barrier properties, is also probable.

These elements include bismuth and lead, whose ions (Bi^{3+}) and (Pb^{2+}) have lone electron pair (LEP) of p-electrons on the outer shell of chalcogen atoms whose energy levels fill the top of the valence band. In particular, the energy states of these pairs determine the features of photoinduced processes and switching and memory effects in chalcogenide glasses. LEP affects the shape of molecules and the structure of the crystal lattice, as it has a strong repulsive effect on the neighboring pairs of electrons involved in the bond architecture as well as on other lone pairs. The appearance of the dominant electronic type of conduction is obviously associated with a sharp increase in the mobility of electrons with respect to the mobility of holes. An increase in the mobility of nonequilibrium holes upon modification of As_2Se_3 with bismuth and lead is also evidenced by a decrease in the activation energy of photoconductivity. An analysis of the structural features of the ChGS group under study revealed the essential role of the LEP both in the implementation of the disordered structure and in the formation of the energy structure of local states (Chaudhary et al. 2020). Based on the analysis of the known literature data and comparison of the latter with the experimental results obtained in the course of the study, it can be concluded that defective valence states of the LEP type play a significant role in the process of electric transport.

Conclusions

The temperature dependences of the conductivity of modified As_2Se_3, As_2S_3<Pb> chalcogenide glasses reveal its thermally activated nature. An increase and a sharp decrease in the activation energy with an increase in the level of ChGS modification are associated with the probable formation of solid solutions upon incorporation of modifier (Pb) atoms into the main glass matrix with a simultaneous decrease in the band gap. Compounds that are close to stoichiometric have a larger E_A value for the As-Se system and a smaller one for As-S. An increase in the activation energy of conduction with a change in the composition in the series As_2Se_3...AsSe correlates with the variation in the height of the potential barrier to the metal—the ChGS boundary. There is a field dependence of the conductivity, which can be interpreted within the framework of the current theory, limited by the space charge of a uniform distribution of local states. The results obtained indicate an increase in the proportion of the electronic component of conductivity and suggest the development of additional mechanisms of electrical transport. The study of amorphous compounds of the modified ChGS type encounters fundamental difficulties due to the difficulty of obtaining samples of a stable and accurate composition due to their tendency to form structures, the disordering of which is largely due to the presence of LEP.

The experimental studies carried out in this work make it possible, to a certain extent, to fill some gap in the study of ChGS electrical properties as well as to expand the scope of their practical application as base materials for electronics with improved performance.

Conflict of Interest

The author declares that there is no conflict of interest, either existing or potential.

References

Chaudhary, S., Modgil, V., Rangra, V. S. (2020) Effect of compositional variation on physical parameters of quaternary chalcogenide glasses $Se_{69}Sn_{10}Ge_{21-x}Sb_x$ ($6 \le x \le 14$). *Journal of Ovonic Research*, 16 (1), 41–52. (In English)

Chirita, A., Prilepov, V. (2022) Chalcogenide glassy semiconductors of the system As-Se-S-Sn for X-ray imaging. *Chalcogenide Letters*, 19 (6), 439–445. (In English)

Chu, J., Sher, A. (2007) *Physics and properties of narrow gap semiconductors*. New York: Springer Publ., 606 p. https://doi.org/10.1007/978-0-387-74801-6 (In English)

Ghayebloo, M., Tavoosi, M., Rezvani, M. (2017) Compositional modification of Se-Ge-Sb chalcogenide glasses by addition of arsenic element. *Infrared Physics & Technology*, 83, 62–67. https://doi.org/10.1016/j.infrared.2017.04.010 (In English)

Gubanov, A. I. (1963) *Kvantovo-elektronnaya teoriya amorfnykh provodnikov [Quantum-electronic theory of amorphous conductors]*. Moscow; Leningrad: USSR Academy of Sciences Publ., 250 p. (In Russian)

Kazakova, L. P., Lebedev, E. A. (1998) Effect of metal impurities on the drift mobility of charge carriers in glassy chalcogenide semiconductors. *Semiconductors*, 32 (7), 714–715. https://doi.org/10.1134/1.1187490 (In English)

Kolomiets, B. T., Averianov, V. L., Lyubin, V. M., Prikhodko, O. J. (1982) Modification of vitreous As_2Se_3. *Solar Energy Materials*, 8 (1-3), 1–8. (In English)

Mehta, N. (2006) Applications of chalcogenide glasses in electronics and optoelectronics: A review. *Journal of Scientific and Industrial Research*, 65 (10), 777–786. (In English)

Moynihan, C. T., Gavin, D. L., Syed, R. (1982) Pre-exponential term in the Arrhenius equation for electrical conductivity of glass. *Journal de Physique Colloques*, 43 (C9), C9-395–C9-398. https://doi.org/10.1051/jphyscol:1982975 (In English)

Nardone, M., Simon, M., Karpov, I. V., Karpov, V. G. (2012) Electrical conduction in chalcogenide glasses of phase change memory. *Journal of Applied Physics*, 112 (7), article 071101. https://doi.org/10.1063/1.4738746 (In English)

Nguyen, H. T., Yakubov, A. O., Lazarenko, P. I. et al (2018) Characteristics of amorphous As_2S_3 semiconductor films obtained via spin coating. *Semiconductors*, 52 (15), 1963–1968. https://doi.org/10.1134/S1063782618150058 (In English)

Zhang, X. G., Pantelides, S. T. (2012) Theory of space charge limited currents. *Physical Review Letters*, 108 (26), article 266602. https://doi.org/10.1103/PhysRevLett.108.266602 (In English)

Physics of Semiconductors. Physics of thin films

UDC 538.935

EDN TFGFTE
https://www.doi.org/10.33910/2687-153X-2023-4-2-75-80

Effect of a transverse electric field on the resistance of thin films of the $Bi_{1-x}Sb_x$ (x = 0–0.12) system on mica

V. M. Grabov[1], V. A. Komarov[1], S. V. Pozdnyakov✉[1], V. A. Gerega[1], A. V. Suslov[1]

[1] Herzen State Pedagogical University of Russia, 48 Moika Emb., Saint Petersburg 191186, Russia

Authors

Vladimir M. Grabov, ORCID: 0000-0003-0215-6474, e-mail: vmgrabov@yandex.ru

Vladimir A. Komarov, ORCID: 0000-0002-2482-0885, e-mail: va-komar@yandex.ru

Stepan V. Pozdnyakov, ORCID: 0000-0002-8319-1492, e-mail: stepan.pozdnyakov.98@mail.ru

Vasilisa A. Gerega, ORCID: 0000-0003-4235-7713, e-mail: gerega.vasilisa96@gmail.com

Anton V. Suslov, ORCID: 0000-0003-1934-245X, e-mail: a.v_suslov@mail.ru

For citation: Grabov, V. M., Komarov, V. A., Pozdnyakov, S. V., Gerega, V. A., Suslov, A. V. (2023) Effect of a transverse electric field on the resistance of thin films of the $Bi_{1-x}Sb_x$ (x = 0–0.12) system on mica. *Physics of Complex Systems*, 4 (2), 75–80. https://www.doi.org/10.33910/2687-153X-2023-4-2-75-80 EDN TFGFTE

Received 1 March 2023; reviewed 7 April 2023; accepted 7 April 2023.

Funding: This study was supported by the Ministry of Education of the Russian Federation as part of the state-commissioned assignment (project No. VRFY-2023-0005).

Abstract. The paper is devoted to the study of transverse electric field effect on transport properties of charge carriers in bismuth and bismuth-antimony thin films. Experimental results reveal the existence of electric field effect in thin films of composition up to 12 at.% Sb. The dependencies of resistance on magnitude of electric field are obtained in a wide range of film thicknesses. A qualitative interpretation of the observed effect is given based on the analysis of the mobility of electrons and holes in films depending on the sign of the electric field and the film thickness.

Keywords: bismuth, bismuth-antimony, thin films, electric field effect, mica substrate

Introduction

The electric field effect (EFE) in semiconductors has been well studied. The EFE is a powerful tool for changing the electronic properties of near-surface layers of a semiconductor. At present, this effect underlies the technology of metal-dielectric-semiconductor silicon microelectronics.

It is of interest to use the EFE to change the electronic properties of semimetals—bismuth and its alloys with antimony. Taking into account the features of the energy spectrum of charge carriers in bulk semimetals and its thin films (Chang et al. 2019; Ferreira 1968; Jezequel et al. 1997), EFE can lead to new effects.

EFE in semimetals has not been practically studied until now. There are several works on the study of EFE in bismuth films (Butenko et al. 1997; 1999; 2000; Hong et al. 2020). However, the information presented there does not allow one to obtain a complete picture of the manifestation of this effect in semimetals. The factors listed above led us to study EFE in semimetal films.

The paper presents the results of the study of EFE on the resistance of bismuth and bismuth-antimony (with antimony content 0, 3, 5, 8, and 12 at.%) films on thin mica substrate.

Experimental methods

The bismuth and bismuth-antimony thin films were produced by vacuum thermal deposition in a vacuum up to 10^{-5} Torr in the thickness range of 50–1000 nm. Bismuth-antimony films were produced using discrete thermal evaporation. The use of this method ensures a uniform distribution of antimony over the volume of the film. Muscovite mica 20–40 μm thick was used as a substrate.

The films were deposited on the substrate at a temperature of 120 °C and subsequently annealed at a temperature of 250 °C. The annealing duration was 30 min. The film deposition modes ensure the obtaining of large-block films on a mica substrate (the block sizes are much larger than the film thickness). Producing films with uniform block sizes is important, since it was shown that block size significantly affects the transport properties of charge carriers in semimetal films (Komarov et al. 2019).

The crystal structure was studied by atomic force microscopy (AFM) and Xray diffraction (XRD) using the equipment of Herzen University interdisciplinary core facilities. The study shows that the crystallographic orientation of the film crystal is such that the (111) plane of the crystal is parallel to the film plane, which is typical for bismuth films (Grabov et al. 2020; Krushelnitckii et al. 2017).

The study of the influence of the transverse electric field on the resistance of the film was carried out on a capacitor structure (Fig. 1). In this structure, the substrate was a dielectric, on one side of which a semi-metallic film was deposited and on the other side there was a metal field electrode. Contact pads were deposited on the edges of the film to carry out electrical measurements. The field electrode corresponds to cover only the active part of the bismuth film. The geometric dimensions of the active part of the film were as follows: the width was 1 mm and the length was 0.5 mm. The measurements were carried out at a direct current through the films and an alternating voltage at the field electrode. This made it possible to directly measure the change in the film resistance as a function of the potential at the field electrode and increase the accuracy and repeatability of the results obtained. The measurements were made in the frequency range 50–200 Hz. The polarity of the control field was determined from the polarity of the field electrode, i. e., positive polarity means that the film under study is negatively charged. The measurements were carried out at temperatures of 300 K and 77 K.

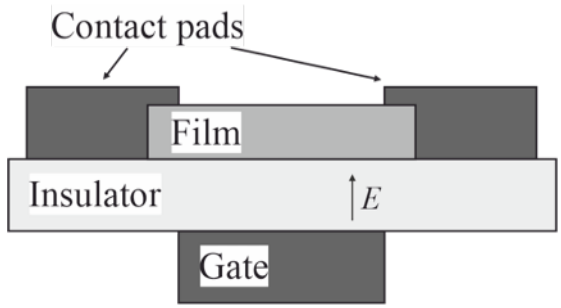

Fig. 1. Scheme of samples capacitor structure

Experimental results

Fig. 2 illustrates the results of the study regarding the EFE on the resistance of $Bi_{0.97}Sb_{0.03}$ films of various thicknesses. As can be seen from Fig. 2, the dependence of the resistance on the transverse field changes significantly with the film thickness. In films of large thickness, it has a non-linear character, both with positive and negative polarity at the field electrode. In $Bi_{0.97}Sb_{0.03}$ films, at a positive potential at the field electrode, an increase in the film resistance is observed with increasing field strength. The relative magnitude of the change increases with decreasing film thickness. With a negative polarity on the field electrode, the resistance of films with a thickness of 50 nm and 100 nm decreases. In thicker films, the dependence has a minimum. The position of the minimum shifts to the region of higher field strength with decreasing film thickness. Thus, for a 250 nm film, only the minimum is reached, but there is no increase in resistance within the limits of the achievable control field strength. A similar character of the dependences is also observed in films of pure bismuth.

 https://www.doi.org/10.33910/2687-153X-2023-4-2-75-80

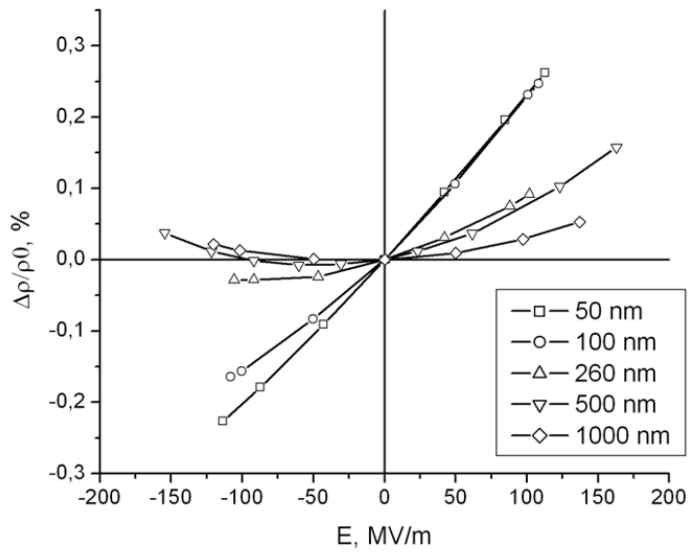

Fig. 2. Relative change in the resistance of $Bi_{0.97}Sb_{0.03}$ films of different thicknesses on the electric field strength at T =77 K

With an increase in antimony concentration, the observed dependences change in form. As an illustration, Fig. 3 shows similar dependences for $Bi_{0.92}Sb_{0.08}$ films. Comparison of the results shown in Fig. 2 and Fig. 3 reveals significant differences between them. For 500 nm thick films, the dependences qualitatively coincide in shape. For 250 nm films, the dependences change qualitatively: in $Bi_{0.97}Sb_{0.03}$ films, the resistance minimum is observed at negative polarity, while in the $Bi_{0.92}Sb_{0.08}$ film, it passes into the region of positive polarity at the field electrode. In 50 and 100 nm $Bi_{0.92}Sb_{0.08}$ films, the sign of the effect is opposite to that of the $Bi_{0.97}Sb_{0.03}$ films. A further increase in the concentration of antimony in the films leads to the fact that for films in the entire range of thicknesses, a decrease in resistance is observed at a positive potential at the field electrode.

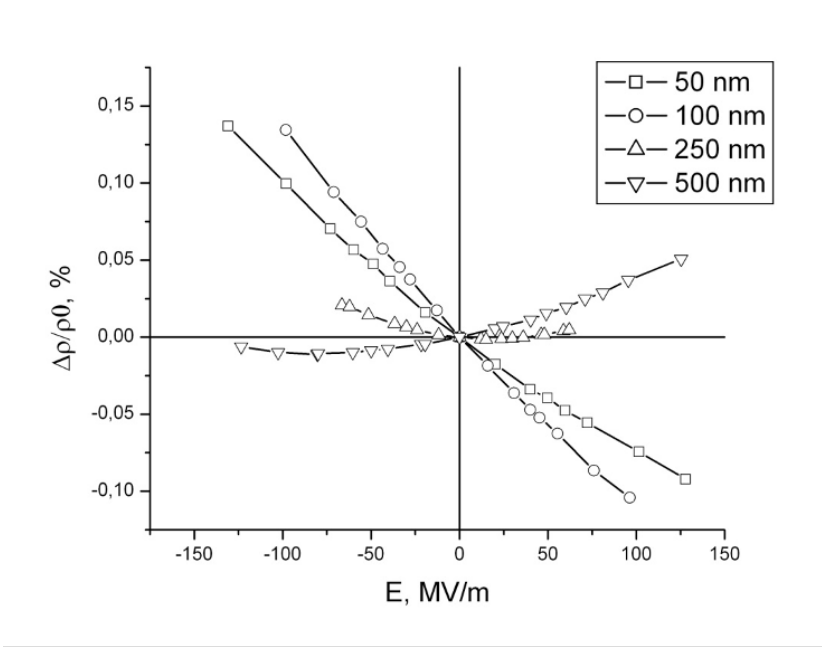

Fig. 3. Relative change in the resistance of $Bi_{0.92}Sb_{0.08}$ films of different thicknesses on the electric field strength at T =77 K

When comparing the dependences of the film resistance on the field strength of films of various compositions of the same thickness of 50 nm, two types of dependences can be distinguished (Fig. 4). The first type includes films of pure Bi, and bismuth-antimony 3 at.% and 5 at.% Sb, in which the resistance increases at positive polarity. The second type includes films of bismuth-antimony 8 at.% Sb and 12 at.% Sb, in which the resistance decreases at positive polarity of the field electrode. A similar trend is also preserved in thicker films.

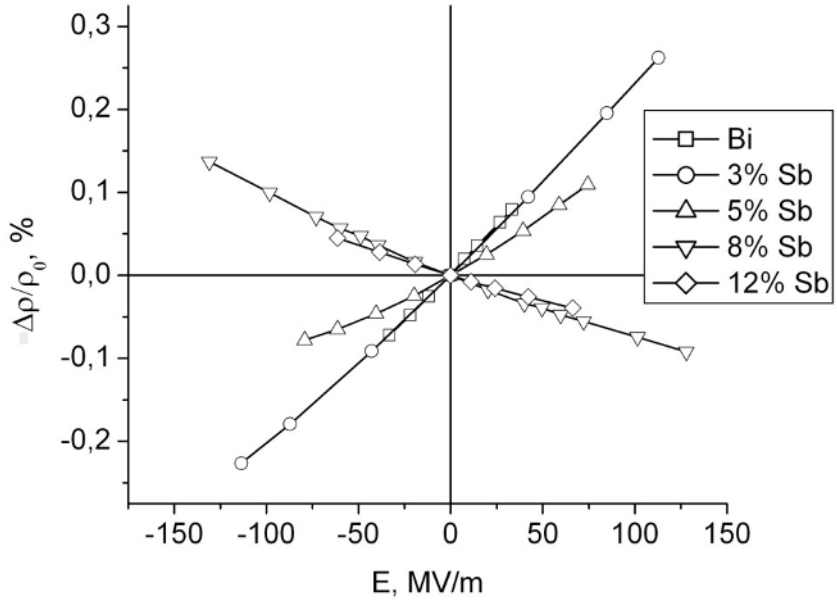

Fig. 4. Relative change in the resistance of 50 nm thick films with different antimony content on the electric field strength at T = 77K

To characterize the magnitude of the effect, we used the coefficient

$$B = \frac{(R - R_0)}{R_0 E}$$

Table 1 lists the values of the coefficient *B* for 50 nm films of various compositions. Films with a thickness of 50 nm were chosen to estimate the magnitude of the effect primarily because, for these films, the dependence of the resistance on the magnitude of the electric field strength is closest to linear, i. e., coefficient *B* is a constant value.

Table 1. The value of the coefficient *B* for 50 nm thick films of various compositions at 77 K

	Bi	**3 at.% Sb**	**5 at.% Sb**	**8 at.% Sb**	**12 at.% Sb**
B,10^{-3} %/MV/m	2.29	2.17	1.23 (1.48)	–0.878	–0.665

An increase in the film thickness leads to the fact that the dependence of the resistance on the field strength ceases to be linear, i.e., coefficient *B* ceases to be a constant value and its value decreases. In the studied films, the greatest deviation from the linear dependence is observed when the sign of the potential at the gate electrode corresponds to the resistance decreases: it is a negative potential for Bi films, 3 at.% and 5 at.% Sb, and a positive potential for films of 8 at.% and 12 at.% Sb.

 https://www.doi.org/10.33910/2687-153X-2023-4-2-75-80

Discussion

Before a discussion of the results obtained is started, it should be noted that the EFE in semimetals is fundamentally different from the effect in semiconductors. In semiconductors, the concentration of intrinsic charge carriers is very low, and free charge carriers are due to the ionization of dopant atoms. This leads to the fact that regions depleted of free-charge carriers can exist in the semiconductor. In semimetals, even at $T = 0$ K, the concentration of free charge carriers is nonzero. For example, in bismuth at $T = 4.2$ K, the concentration of free charge carriers is 3×10^{23} 1/m^3. This fact makes it impossible to create regions with low electrical conductivity; one can only slightly increase or decrease it. Charging a semimetallic electrode leads to an increase in the concentration of one type of carriers and a decrease in the concentration of another type of charge carriers. The total concentration of charge carriers changes insignificantly. This suggests that the change in electrical conductivity is associated with the difference in the mobility of charge carriers of different signs and its change—with a change in the concentration of these charge carriers.

In thin semimetal films, the mobility of charge carriers is largely determined by the action of the classical size effect. As shown in (Komarov et al. 2019), the thickness of the film reduces the electron mobility to a greater extent than the mobility of the holes, and the block sizes reduce the mobility of the holes more strongly. This leads to a change in the ratio of the mobility of electrons and holes in films of different thicknesses and with different block sizes.

A change in the antimony content in the alloy leads to a change in the band structure of the alloy. The ongoing changes in the band structure lead to a decrease in the contribution of holes to galvanomagnetic effects: the Hall coefficient of the films is 8 at. % and 12 at.% Sb has a negative sign over the entire temperature range and for all film thicknesses (Grabov et al. 2017). For example, Fig. 5 shows the dependences of the Hall coefficient on temperature for films of various compositions with a thickness of 1 μm.

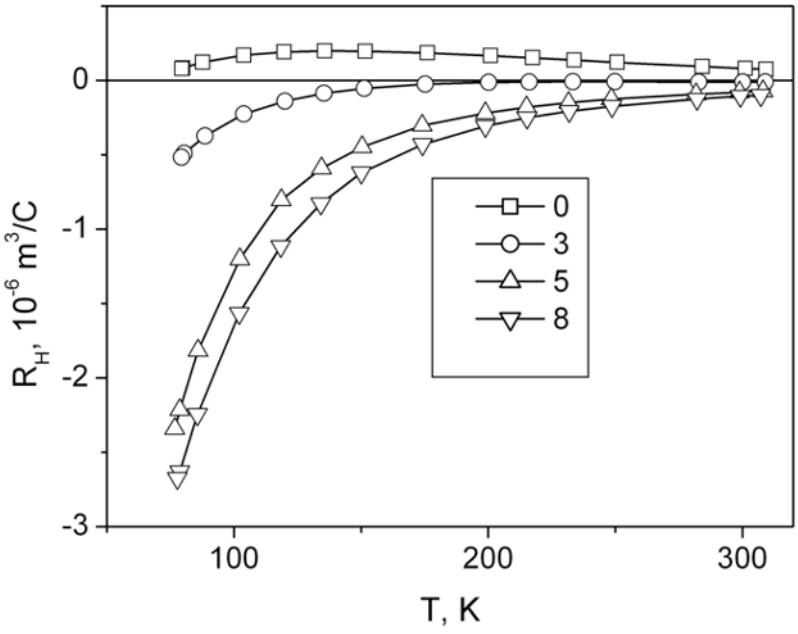

Fig. 5. Temperature dependence of the Hall coefficient of films of various compositions (0–8 at.% Sb) with a thickness of 1 μm (Grabov et al. 2017)

Accounting for the above facts, we can explain the observed experimental dependences as follows. Consider, for example, films of pure bismuth. When a positive potential is applied to the field electrode, the film becomes negatively charged; it increases the concentration of electrons and decreases the concentration of holes. Considering that in a bismuth film with a large block size, the mobility of holes is higher than that of electrons, such an increase in the electron concentration leads to an increase in the resistance of the film. The change of polarity at the field electrode leads to the enrichment

of the film with holes and the depletion of electrons. At the initial stage, this leads to a decrease in the resistance of the film. With an increase in the excess concentration of holes, the resistance increases.

The position of the minimum resistance of the film depends on the initial ratio of the mobility of electrons and holes in the film. This ratio strongly depends on the action of the size effect, and hence on the film thickness.

Conclusions

The study experimentally confirmed the existence of an EFE in thin films of bismuth and bismuth-antimony alloys up to 12 at.% Sb. The dependence of the magnitude of the EFE on the thickness of the films was obtained: with a decrease in the thickness of the film, the magnitude of the effect increases. The dependence of the magnitude and sign of the effect on the concentration of antimony in the alloy is obtained. A qualitative interpretation of the observed effect and its change is given.

Conflict of Interest

The authors declare that there is no conflict of interest, either existing or potential.

Author Contributions

Vladimir Grabov—data analysis, editing, supervision; Vladimir Komarov—development of the setup for measuring the EFE in thin films, data analysis, editing, supervision; Stepan Pozdnyakov—measurements of the EFE in thin films; Vasilisa Gerega—sample production, preparation of the manuscript and figures; Anton Suslov—XRD and AFM measurements. All authors have read and agreed to the published version of the manuscript.

References

Butenko, A. V., Sandomirsky, V., Schlesinger, Y., Shvarts, Dm. (1997) Characterization of the electrical properties of semimetallic Bi films by electrical field effect. *Journal of Applied Physics*, 82 (3), 1266–1273. https://doi.org/10.1063/1.365897 (In English)

Butenko, A. V., Shvarts, Dm., Sandomirsky, V., Schlesinger, Y. (1999) The cause of the anomalously small electric field effect in thin films of Bi. *Applied Physics Letters*, 75 (11), 1628–1630. https://doi.org/10.1063/1.124776 (In English)

Butenko, A. V., Shvarts, Dm., Sandomirsky, V., Schlesinger, Y. (2000) Quantum-size oscillations of the electric field effect (EFE) in thin Bi films. *Physica B: Condensed Matter*, 284–288, 1942–1943. https://doi.org/10.1016/S0921-4526(99)03059-8 (In English)

Chang, T.-R., Lu, Q., Wang, X. et al. (2019) Band topology of bismuth quantum films. *Crystals*, 9 (10), article 510. https://doi.org/10.3390/cryst9100510 (In English)

Ferreira, L. G. (1968) Band structure calculation for bismuth: Comparison with experiment. *Journal of Physics and Chemistry of Solids*, 29 (2), 357–365. https://doi.org/10.1016/0022-3697(68)90081-4 (In English)

Grabov, V. M., Gerega, V. A., Demidov, E. V. et al. (2020) On the atomic-force microscopy and electrical properties of single-crystal bismuth films. *Journal of Surface Investigation: X-ray, Synchrotron and Neutron Techniques*, 14 (5), 913–917. https://doi.org/10.1134/S1027451020050055 (In English)

Grabov, V. M., Komarov, V. A., Demidov, E. V. et al. (2017) Temperature dependences of galvanomagnetic coefficients of bismuth-antimony thin films 0–15 at.% Sb on substrates with different temperature expansion. *Universitetskij nauchnyj zhurnal — Humanities & Science University Journal*, 35, 48–57. EDN: DCTMQP (In English)

Hong, L.-C., Chou, C., Lin, H.-H. (2020) Simulation on the electric field effect of Bi thin film. *Solid State Electronics Letters*, 2, 28–34. https://doi.org/10.1016/j.ssel.2020.04.001 (In English)

Jezequel, G., Thomas, J., Pollini, I. (1997) Experimental band structure of semimetal bismuth. *Physical Review B*, 56 (11), 6620–6626. https://doi.org/10.1103/PhysRevB.56.6620 (In English)

Komarov, V. A., Grabov, V. M., Suslov, A. V. et al. (2019) The Hall and Seebeck effects in bismuth thin films on mica substrates in the temperature range of 77–300 K. *Semiconductors*, 53 (5), 593–598. https://doi.org/10.1134/S1063782619050105 (In English)

Krushelnitckii, A. N., Demidov, E. V., Ivanova, E. K. et al. (2017) Dependence of the surface morphology of ultrathin bismuth films on mica substrates on the film thickness. *Semiconductors*, 51 (7), 876–878. https://doi.org/10.1134/S1063782617070211 (In English)

Physics of Semiconductors. Physics of thin films

UDC 538.9 + 537.9

EDN VSFWYN
https://www.doi.org/10.33910/2687-153X-2023-4-2-81-87

Spherulitic microstructure of thin PZT films

V. P. Pronin[✉1], S. V. Senkevich[1,2], A. S. Elshin[3], E. D. Mishina[3], I. P. Pronin[2]

[1] Herzen State Pedagogical University of Russia, 48 Moika Emb., Saint Petersburg 191186, Russia
[2] Ioffe Institute, 26 Polytechnicheskaya Str., Saint Petersburg 194021, Russia
[3] Russian Technological University MIREA, 78 Vernadskogo Ave., Moscow 119454, Russia

Authors

Vladimir P. Pronin, ORCID: 0000-0003-0997-1113, e-mail: pronin.v.p@yandex.ru

Stanislav V. Senkevich, ORCID: 0000-0002-4503-1412, e-mail: senkevichSV@mail.ioffe.ru

Andrey S. Elshin, ORCID: 0000-0002-0037-7137, e-mail: elshin_andrew@mail.ru

Elena D. Mishina, ORCID: 0000-0003-0387-5016, e-mail: mishina_elena57@mail.ru

Igor P. Pronin, ORCID: 0000-0003-3749-8706, e-mail: petrovich@mail.ioffe.ru

For citation: Pronin, V. P., Senkevich, S. V., Elshin, A. S., Mishina, E. D., Pronin, I. P. (2023) Spherulitic microstructure of thin PZT films. *Physics of Complex Systems*, 4 (2), 81–87. https://www.doi.org/10.33910/2687-153X-2023-4-2-81-87 EDN VSFWYN

Received 27 March 2023; reviewed 21 April 2023; accepted 21 April 2023.

Funding: This study was supported by the Ministry of Education of the Russian Federation as part of the state-commissioned assignment (project No. VRFY-2023-0005).

Abstract. The paper shows that the formation of a radiant spherulites microstructure in lead zirconate-titanate thin films obtained by radio-frequency magnetron sputtering is associated with the formation of radial tensile mechanical stresses acting in the substrate plane, the magnitude of which increases with increasing linear size of spherulites. It leads to a change in the lattice parameter of the perovskite structure and the appearance of induced polarization, the value of which can significantly exceed the spontaneous polarization.

Keywords: PZT thin films, spherulitic microstructure, optical second harmonic generation, mechanical stresses, induced polarization

Introduction

Around us, spherulitic crystal structures are widespread in the organic and inorganic nature. The first works on the study of their structure and formation mechanisms were started in the first half of the 19th century by Talbot, Brewster (Brewster 1815; 1853; Talbot 1837) and somewhat later by a number of other researchers (Cross 1891). The types of spherulitic structures are well classified and vary greatly in growth pattern and microstructure. Spherulites are widely represented in minerals, as a rule, in the form of balls of a radially radiant structure (Kantor 1997; Shtukenberg et al 2012).

The current attention to spherulites is associated, in particular, with the development of miniature piezoelectric quartz oscillators, which require the use of thin-film technologies for their manufacture (Lutjes et al. 2021; Musterman et al. 2022). Practice has shown that the process of crystallization of quartz films from a glassy phase is difficult to control, and the films themselves often take the form of radiant spherulites (Lutjes et al. 2021; Musterman et al. 2022). As experiments have shown, one of the features of radiant spherulites is the rotation of the growth axis during the radial growth of spherulites (from the center to the periphery), which leads to structural disturbances and, apparently, negatively affects the oscillatory properties of the grown films.

It turned out that the spherulitic microstructure is widespread in thin polycrystalline films, including lead zirconate titanate (PZT) films (Alkoy et al. 2007; Klee et al. 1994; Preston, Haertling 1992; Pronin et al. 2018), which are increasingly used in microelectromechanical and infrared technology devices (Izyumskaya et al. 2007; Muralt et al. 2009; Song et al. 2021). However, there are practically no studies of the influence of the microstructure of films on their physical properties. The relevance of these studies is evidenced, however, by the fact that in thin PZT films in a narrow region of the morphotropic phase boundary (MPB), anomalously high electromechanical and piezoelectric parameters are observed, and it is obvious that a change in the microstructure of films can most decisively affect their physical characteristics. We carried out the first studies in this direction in previous years and found anomalous changes in the signal of the second optical harmonic (Elshin et al. 2020) and changes in the dielectric characteristics (Dolgintsev et al. 2021). The purpose of this work was to elucidate the possible causes of such anomalies in thin films of PZT.

Sample preparation and research methods

Samples of thin films were obtained using a two-stage method of radio-frequency magnetron sputtering and varying the distance from the target to the substrate. The substrate was a platinized silicon wafer. The thickness of the PZT films was nearly 500 nm, and the composition corresponded to the MPB region. In our previous works (Dolgintsev et al. 2021; Elshin at al. 2020), the technology for obtaining samples is described in more detail. Both single-phase perovskite films formed at 580 °C and films formed at 550 °C in which islands of the perovskite phase were formed in the matrix of the low-temperature pyrochlore phase were prepared.

To study the phase state, microstructure, and physical properties of thin films, we used a scanning electron microscope (SEM, EVO-40, Zeiss), an optical microscope Nikon Eclipse LV 150 as well as the method of nonlinear optical microscopy, which is informative for studying phase transitions and domain structures. The method is based on the analysis of the second optical harmonic signal (SHG), which is proportional to the square of the ferroelectric polarization oriented normally to the direction of propagation of the incident optical beam (Wang et al. 2017).

The second optical harmonic was excited by femtosecond laser radiation with a wavelength of 800 nm, a repetition rate of 80 MHz, and a duration of 100 fs. The SHG intensity was recorded at a wavelength of 400 nm. The plane of polarization of the incident beam was rotated by a half-wave plate in front of the sample. A Glan prism was used as an analyzer. The images were fixed in the "reflection" geometry. The Zeiss N-achroplan 100X objective of the WITec alpha 300S confocal microscope provided a spot on the sample with a diameter of 0.9 μm, and the use of an optical fiber provided a spatial resolution of ~300 nm.

Experimental results and discussion

Images of individual perovskite islands are shown in Fig. 1. Fig. 1a is a SEM image obtained in the backscattered electron mode (the energy of the incident beam is 12 keV), and Figs. 1b and 1c are SHG images obtained for two polarization directions of the incident beam, differing by 90 degrees. It can be seen that the perovskite islands are almost round in shape and are characterized by a radially radiant spherulitic microstructure. The microstructure of the inner part of the spherulite strongly differs from the periphery. This difference is especially pronounced in SHG images, where the boundary between these regions is clearly visible.

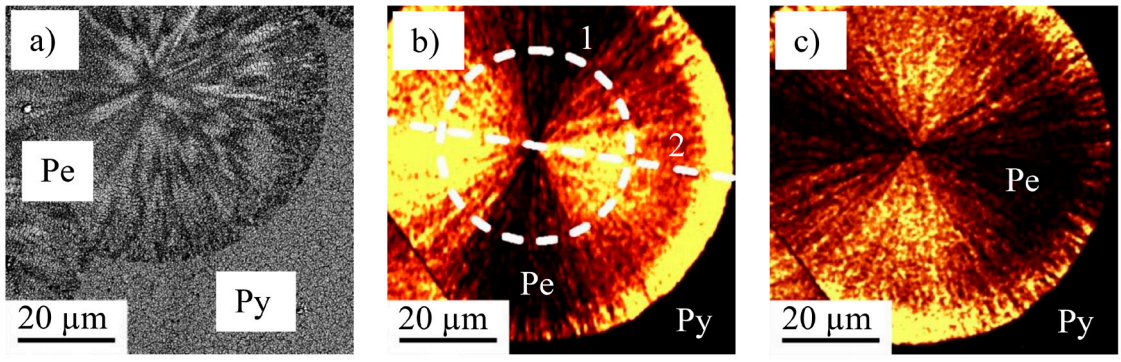

Fig. 1. SEM (a) and nonlinear optical images (b, c) of perovskite (Pe) islands in a pyrochlore (Py) matrix. Dotted lines in Fig. 1b show the diametrical and circular cross sections (1, 2)

 https://www.doi.org/10.33910/2687-153X-2023-4-2-81-87

Fig. 2 is a diametrical cross section (line 1 in Fig. 1b) of the distribution of the SHG signal. Its value increases at the edges of the spherulite by a factor of ~2 compared to the signal in the central region. This behavior may indicate the formation of a radially radiant microstructure during the crystallization of the perovskite phase from the low-temperature pyrochlore phase through the intermediate perovskite phase, which is characterized by lower density. A similar nature of the recrystallization of the perovskite phase was observed earlier for perovskite spherulites, which differ in stepwise growth (Pronin et al. 2010).

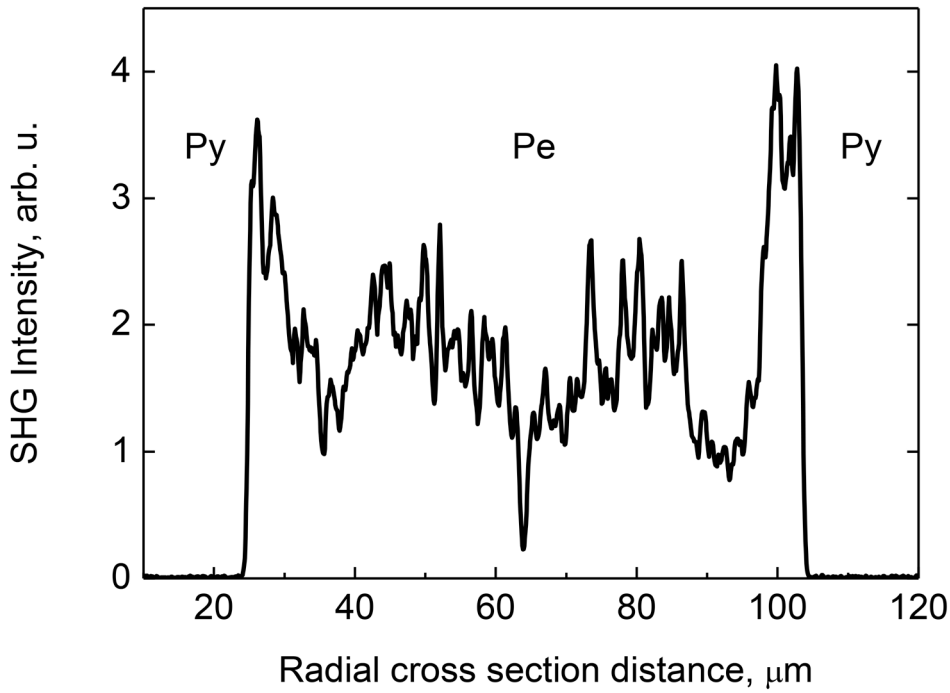

Fig. 2. Distribution of the SHG signal over section 1 in Fig. 1b spherulitic island

A distinct drop in the SHG signal at the interface between two modifications of perovskite phases (dense and loose) indicates that either the growth orientation and, as a consequence, the polarization orientation (with respect to the film plane) can differ greatly in these phases, while maintaining the same spatial symmetry of the ferroelectric phase, or the boundary is the region of phase transformation of the ferroelectric phase. So far, this question has not been answered and requires further research.

In Fig. 2, attention is also drawn to the near-sinusoidal change in the SHG signal, at which the signal is minimal in the center of the island, then, when moving away from the center, it first increases, reaching a local maximum approximately at the middle of the radius, and then decreases towards the edge. In other words, there is a radial "rotation" of the polarization vector. According to the results of the recent studies, in radiant spherulites, a rotation of the growth axis is observed with increasing spherulite radius (Elshin et al. 2023; Lutjes et al. 2021), which can lead to a change in the lateral polarization projection. However, additional studies are also required to confirm this assumption.

Fig. 3 reflects the change in the SHG signal over the circular cross section (marked by number 2 in Fig. 1b) for two directions of linear polarization of the incident beam, which differ by 90 degrees. It can be seen that the circular cross sections for a fixed polarization direction have two maxima. The obtained result suggests a correlation between the orientation of the polarization of the incident optical radiation and the orientation of the polarization vector in a ferroelectric film.

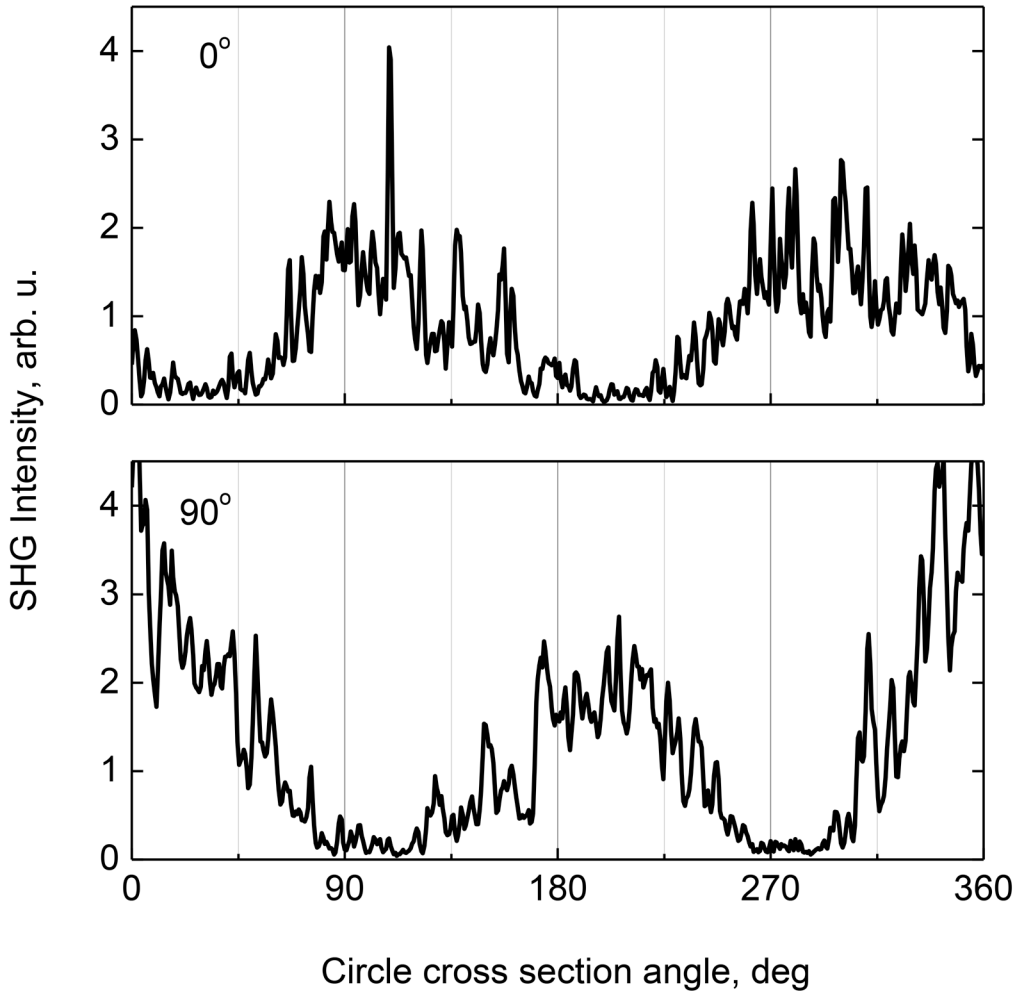

Fig. 3. Distribution of the SHG signals over circular section 2 (Fig. 1b) of a spherulite island of the incident beams with linear polarization differing by 90 °C

The observed result suggests that the cause of the collinearity of the optical polarization vector and the polarization vector in the spherulite may be radial mechanical stresses during the growth of the spherulite island. According to (Kukushkin et al. 2012), such radial mechanical stresses are caused by the difference in the density of the perovskite and pyrochlore phases at perovskite phase crystallization. Since the density of the pyrochlore phase is lower than the density of the perovskite phase, the perovskite island will be subjected to radial tension from the side of the pyrochlore matrix, which will lead to the appearance of a mechanically induced radially oriented polarization. Thus, the observed increase in the SHG signal at the periphery of the spherulitic island can be associated with a greater susceptibility to polarization reorientation in the region of the porous periphery relative to the denser central part of the island.

On Fig. 4, the left column shows the SHG images, and the right column shows the SEM images of single-phase PZT films deposited at different distances from the target to the substrate (at 40 and 70 mm) and different temperatures of the substrate heating by plasma (145 °C and 90 °C, respectively). It is clearly seen that a change in the technological parameters of film deposition leads to significant changes in the size and nature of the microstructure of spherulitic blocks as well as in the SHG signal (Table 1). It can be seen from Table 1 that a decrease in the film deposition temperature leads to a sharp change in the concentration of block spherulites, the number of which increases by almost an order of magnitude, the pseudocubic lattice parameter decreases, and the SHG signal increases by about 20 times.

 https://www.doi.org/10.33910/2687-153X-2023-4-2-81-87

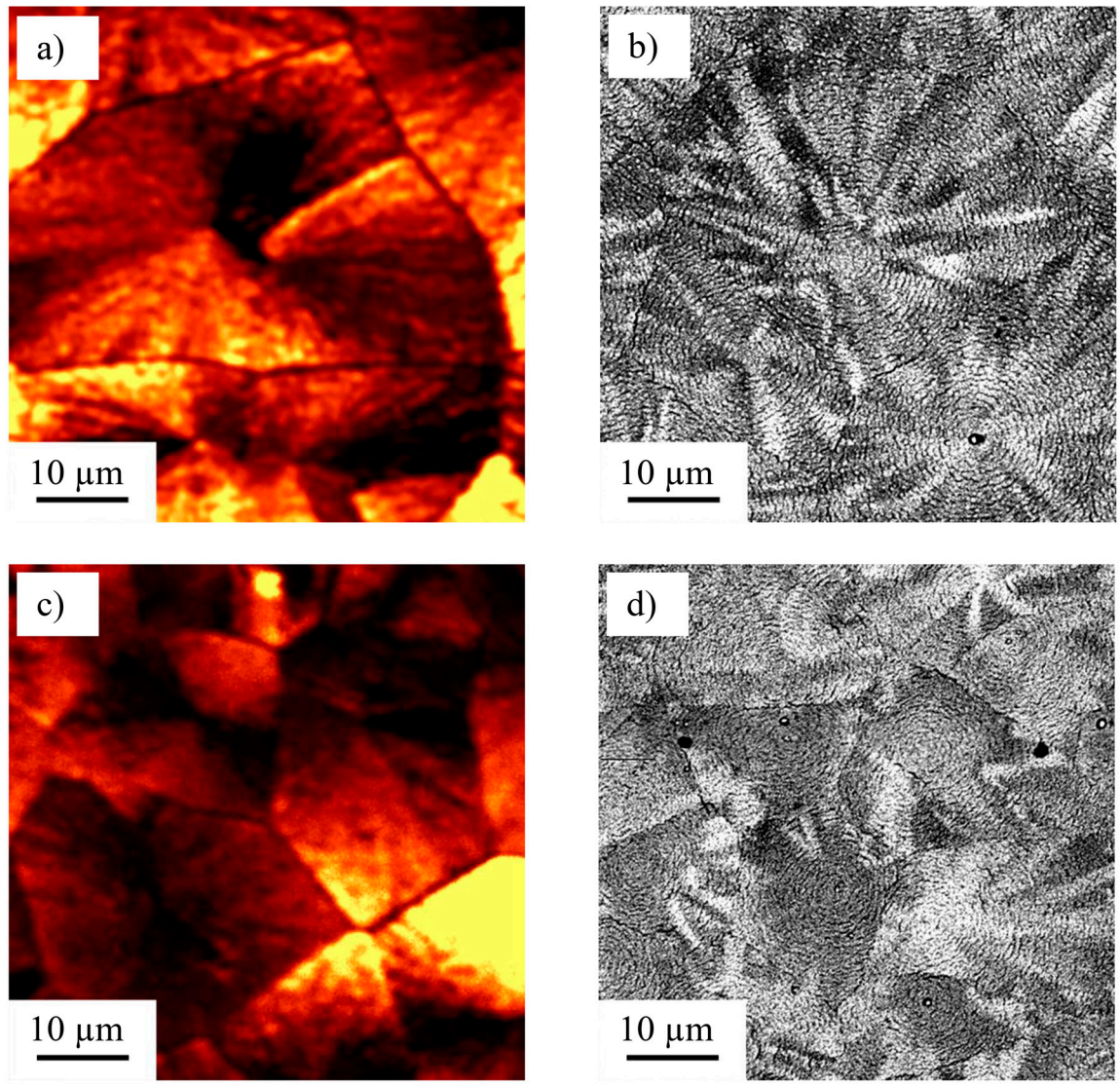

Fig. 4. Nonlinear optical and SEM images of PZT films deposited at different distances from the target to the substrate: d = 30 mm (a, b) and 70 mm (c, d)

Table 1. Changes in a number of technological, structural, and optical parameters of thin PZT films deposited at different distances from the target to the substrate

Distance from substrate to target, mm	Deposition temperature, °C	Block concentration, 10^2/mm^2	SHG signal, relat. un.	Pseudocubic lattice parameter, nm
40	145	9	45	0.40677
70	90	70	17	0.40738

The obtained data suggest that the anomalously high SHG signal in the film obtained at a distance from the target to the substrate of 40 mm is associated with an increase in tensile mechanical stresses, which increase with an increase in the linear dimensions of the spherulite blocks. In turn, these mechanical stresses induce an anomalously high polarization in the film plane, the value of which can be several times greater than the spontaneous polarization characteristic of a PZT film.

Conclusions

The analysis of the results obtained in this work allows us to conclude that in PZT films with a spherulite microstructure, the anomalous SHG signal is induced by radial mechanical stresses, the magnitude of which increases with the linear size of the spherulites. Estimates of the polarization show that it can exceed the spontaneous ferroelectric polarization by several times. It was found that the formation of a radiant spherulitic microstructure with a perovskite structure from a low-temperature nonpolar pyrochlore phase occurs in two stages, with the formation of a loose intermediate perovskite phase.

Conflict of Interest

The authors declare that there is no conflict of interest, either existing or potential.

Authors contribution

The authors have made an equal contribution to the preparation of the paper.

References

Alkoy, E. M., Alkoy, S., Shiosaki, T. (2007) The effect of crystallographic orientation and solution aging on the electrical properties of sol-gel derived $Pb(Zr_{0.45}Ti_{0.55})O_3$ thin films. *Ceramic International*, 33 (8), 1455–1462. https://doi.org/10.1016/j.ceramint.2006.06.010 (In English)

Brewster, D. (1815) III. Experiments on the depolarisation of light as exhibited by various mineral, animal, and vegetable bodies, with a reference of the phenomena to the general principles of polarisation. By David Brewster, LL. D. F. R. S. Edin and F. S. A. Edin. In a letter addressed to the Right Hon. Sir Joseph Banks, Bart. K. B. P. R. S. *Philosophical Transactions*, 105, 29–53. https://doi.org/10.1098/rstl.1815.0004 (In English)

Brewster, D. (1853) XLIII.-On Cricular Crystals. *Earth and Environmental Science. Transactions of the Royal Society of Edinburgh*, 20 (4), 607–623. https://doi.org/10.1017/S0080456800033895 (In English)

Cross, W. (1891) Constitution and origin of spherulites in acid eruptive rocks. *Bulletin of the Philosophical Society of Washington*, 11, 411–502. (In English)

Dolgintsev, D. M., Senkevich, S. V., Kaptelov, E. Yu. et al. (2021) Microstructure and properties of polycrystalline PZT films obtained by RF magnetron sputtering with fine variation of the composition near morphotropic phase boundary. *Physics of Complex Systems*, 2 (3), 101–109. https://www.doi.org/10.33910/2687-153X-2021-2-3-101-109 (In English)

Elshin, A. S., Pronin, I. P., Senkevich, S. V., Mishina, E. D. (2020) Nonlinear optical diagnostics of thin polycrystalline lead zirconate titanate films. *Technical Physics Letters*, 46 (4), 385–388. https://doi.org/10.1134/S1063785020040215 (In English)

Elshin, A. S., Staritsyn, M. V., Pronin, I. P. et al. (2023) Nonlinear optics for crystallographic analysis in lead zirconate titanate. *Coatings*, 13 (2), article 247. https://doi.org/10.3390/coatings13020247 (In English)

Izyumskaya, N., Alivov, Y.-I., Cho, S.-J. et al. (2007) Processing, structure, properties, and applications of PZT thin films. *Critical Reviews in Solid State and Materials Sciences*, 32 (3-4), 111–202. https://doi.org/10.1080/10408430701707347 (In English)

Kantor, B. Z. (1997) *Besedy o mineralakh [Conversations about minerals]*. Moscow: Astrel Publ., 131 p. (In Russian)

Klee, M., de Veirman, A., Taylor, D. J., Larsen, P. K. (1994) Structure-property relations in polycrystalline titanate thin films. *Integrated Ferroelectrics*, 4 (3), 197–206. https://doi.org/10.1080/10584589408017022 (In English)

Kukushkin, S. A., Tentilova, I. Y., Pronin, I. P. (2012) Mechanism of the phase transformation of the pyrochlore phase into the perovskite phase in lead zirconate titanate films on silicon substrates. *Physics of the Solid State*, 54 (3), 611–616. https://doi.org/10.1134/S1063783412030158 (In English)

Lutjes, N. R., Zhou, S., Antoja-Lleonart, J. et al. (2021) Spherulitic and rotational crystal growth of Quartz thin films. *Scientific Reports*, 11, article 14888. https://doi.org/10.1038/s41598-021-94147-y (In English)

Muralt, P., Polcawich, R. G., Trolier-McKinstry, S. (2009) Piezoelectric thin films for sensors, actuators, and energy harvesting. *MRS Bulletin*, 34 (9), 658–664. https://doi.org/10.1557/mrs2009.177 (In English)

Musterman, E. J., Dierolf, V., Jain, H. (2022) Curved lattices of crystals formed in glass. *International Journal of Applied Glass Science*, 13 (3), 402–419. https://doi.org/10.1111/ijag.16574 (In English)

Preston, K. D., Haertling, G. H. (1992) Microstructural investigation of acetate-derived PLZT films. *Integrated Ferroelectrics*, 1 (1), 89–98. https://doi.org/10.1080/10584589208215567 (In English)

Pronin, V. P., Dolgintsev, D. M., Osipov, V. V. et al. (2018) The change in the phase state of thin PZT layers in the region of the morphotropic phase boundary obtained by the RF magnetron sputtering with varying target-substrate distance. *IOP Conference Series: Materials Science and Engineering*, 387, article 012063. https://doi.org/10.1088/1757-899X/387/1/012063 (In English)

Pronin, V. P., Senkevich, S. V., Kaptelov, E. Yu., Pronin, I. P. (2010) Features of the formation of a perovskite phase in thin polycrystalline Pb(Zr,Ti)O_3 films. *Journal of Surface Investigation. X-ray, Synchrotron and Neutron Techniques*, 4, 703–708. https://doi.org/10.1134/S1027451010050010 (In English)

Shtukenberg, A. G., Punin, Yu. O., Gunn, E., Kahr, B. (2012) Spherulites. *Chemical Reviews*, 112 (3), 1805–1838. https://doi.org/10.1021/cr200297f (In English)

Song, L., Glinsek, S., Defay, E. (2021) Toward low-temperature processing of lead zirconate titanate thin films: Advances, strategies, and applications. *Applied Physics Reviews*, 8 (4), article 041315. https://doi.org/10.1063/5.0054004 (In English)

Talbot, W. H. F. (1837) III. On the optical phenomena of certain crystals. *Philosophical Transactions*, 127, 25–27. https://doi.org/10.1098/rstl.1837.0005 (In English)

Wang, J.-S., Jin, K.-J, Gu, J.-X. et al. (2017) Direct evidence of correlation between the second harmonic generation anisotropy patterns and the polarization orientation of perovskite ferroelectric. *Scientific Reports*, 7, article 9051. https://doi.org/10.1038/s41598-017-09339-2 (In English)

Summaries in Russian / Информация о статьях на русском языке

Физика конденсированного состояния

ТЕРМОАКТИВАЦИОННАЯ СПЕКТРОСКОПИЯ ПОЛИМЕРНЫХ ПЛЕНОК ПОЛИЭТИЛЕНА С СОПОЛИМЕРОМ ЭТИЛЕНА С ВИНИЛАЦЕТАТОМ

Галиханов Мансур Флоридович, Карулина Елена Анатольевна, Фомичева Елена Егоровна, Резцов Тихон Вадимович

Аннотация. Приведены результаты исследования полимерных пленок на основе смеси полиэтилена высокого давления (ПЭВД) с сополимером этилена с винилацетатом (СЭВА, сэвилен) методом термостимулированной деполяризации. Отмечено, что на температурных зависимостях токов деполяризации, полученных для образцов с разным содержанием сэвилена, наблюдается один максимум. Сделано предположение, что он соответствует дипольно-сегментальной релаксации, происходящей в полиэтилене высокого давления. Результаты расчета энергий активации, соответствующих этому процессу, позволяют сделать вывод о том, что увеличение доли СЭВА в смеси приводит к облегчению дипольно-сегментальной подвижности, а значит, и к увеличению гибкости полимера.

Ключевые слова: полиэтилен, сополимер этилена с винилацетатом, термостимулированная деполяризация, термоактивационная спектроскопия, дипольно-сегментальная релаксация

Для цитирования: Galikhanov, M. F., Karulina, E. A., Fomicheva, E. E., Reztsov, T. V. (2023) Thermoactivational spectroscopy of polyethylene polymer films with an ethylene-vinyl acetate copolymer. *Physics of Complex Systems*, 4 (2), 47–52. https://www.doi.org/10.33910/2687-153X-2023-4-2-47-52 EDN ZFBEBQ

КОМПЛЕКСНАЯ ДИЭЛЕКТРИЧЕСКАЯ ПРОНИЦАЕМОСТЬ ПЛЕНОК ПВДФ В ДИАПАЗОНЕ ИНФРАНИЗКИХ ЧАСТОТ, ОПРЕДЕЛЕННАЯ МЕТОДОМ РЕЛАКСАЦИОННЫХ КАРТ ТЕРМОСТИМУЛИРОВАННЫХ ТОКОВ

Волгина Елена Алексеевна

Аннотация. В работе показана возможность трактовки результатов термоактивационной спектроскопии полимерных пленок ПВДФ, полученных методом термостимулированных токов фракционной поляризации, в терминах низкочастотной диэлектрической спектроскопии. Приведены результаты исследования температурно-частотных зависимостей компонент комплексной диэлектрической проницаемости в пленках ПВДФ с различной степенью ориентации, полиморфным составом и процентным содержание пор, а также определены параметры электрически активных дефектов, ответственных за релаксационные процессы в исследуемом температурном интервале.

Ключевые слова: пористые пленки, поливинилиденфторид, термоактивационная спектроскопия, диэлектрическая спектроскопия, диэлектрические параметры

Для цитирования: Volgina, E. A. (2023) Complex dielectric permittivity of films in the infra-low frequency range as studied byrelaxation maps of thermally stimulated currents. *Physics of Complex Systems*, 4 (2), 53–58. https://www.doi.org/10.33910/2687-153X-2023-4-2-53-58 EDN YGEOSE

Теоретическая физика

О ТЕМПЕРАТУРЕ ВОЛОСАТЫХ ЧЕРНЫХ ДЫР

Вертоградов Виталий Дмитриевич, Кудрявцев Дмитрий Александрович

Аннотация. Метод гравитационного расщепления представляет собой чрезвычайно полезный инструмент для получения новых решений уравнений Эйнштейна посредством минимальных геометрических деформаций. В данной работе мы рассматриваем волосатые заряженные черные дыры, полученные гравитационным расщеплением, и вычисляем их температуру Хокинга, чтобы сравнить ее со случаем, когда волосы не учитываются. Мы выяснили, что волосы при некоторых условиях параметров черной дыры влияют на температуру Хокинга и могут ее повышать. Мы также выяснили, что температура черной дыры в волосатом случае не зависит от электрического заряда.

Ключевые слова: волосатая черная дыра, температура Хокинга, заряженная черная дыра, гравитационное расщепление, уравнения Эйнштейна

Для цитирования: Vertogradov, V. D., Kudryavtsev, D. A. (2023) On the temperature of hairy black holes. *Physics of Complex Systems*, 4 (2), 59–67. https://www.doi.org/10.33910/2687-153X-2023-4-2-59-67 EDN XBRSNM

Физика полупроводников

ЭЛЕКТРОТРАНСПОРТ В ТОНКИХ МОДИФИЦИРОВАННЫХ ПЛЕНКАХ СЕЛЕНИДА И СУЛЬФИДА МЫШЬЯКА

Аванесян Вачаган Тигранович

Аннотация. В исследованных халькогенидных стеклообразных полупроводников (ХСП) обнаружен эффект влияния модификации на характер температурной зависимости электропроводности. Величина последней увеличивается с уменьшением ширины запрещенной зоны и, соответственно, с увеличением энергии активации. Указанная энергия коррелирует с изменением высоты потенциального барьера на контакте между металлом и халькогенидным стеклообразным полупроводником для различных составов материалов As_2Se_3 и As_2S_3. Отмечена существенная роль одиночной пары электронов, принадлежащей атомам модифицирующей примеси. Пара электронов отвечает за реализацию неупорядоченной и дефектной структуры, а также за формирование энергетической системы локальных состояний, оказывающих влияние на процесс переноса носителей заряда.

Ключевые слова: модификация, проводимость, энергия активации, халькогенидный стеклообразный полупроводник, одиночная электронная пара

Для цитирования: Avanesyan, V. T. (2023) Electric transport in thin modified films of selenide and sulfide of arsenic. *Physics of Complex Systems*, 4 (2), 68–74. https://www.doi.org/10.33910/2687-153X-2023-4-2-68-74 EDN TDFUBE

ВЛИЯНИЕ ПОПЕРЕЧНОГО ЭЛЕКТРИЧЕСКОГО ПОЛЯ НА СОПРОТИВЛЕНИЕ ТОНКИХ ПЛЕНОК СИСТЕМЫ $BI_{1-X}SB_X$ (X = 0–0.12) НА СЛЮДЕ

Грабов Владимир Минович, Комаров Владимир Алексеевич, Поздняков Степан Васильевич, Герега Василиса Александровна, Суслов Антон Владимирович

Аннотация. Работа посвящена исследованию влияния поперечного электрического поля на транспортные свойства носителей заряда в тонких пленках висмута и системы висмут-сурьма. В работе экспериментально подтверждено существование эффекта электрического поля в тонких пленках с содержанием сурьмы до 12 ат.%. Получены экспериментальные зависимости сопротивления от величины электрического поля для пленок разных толщин. Дана качественная интерпретация наблюдаемого эффекта на основе анализа подвижности электронов и дырок в пленках в зависимости от знака напряжённости электрического поля и толщины образцов.

Ключевые слова: висмут, висмут-сурьма, тонкие пленки, эффект электрического поля, подложка из слюды

Для цитирования: Grabov, V. M., Komarov, V. A., Pozdnyakov, S. V., Gerega, V. A., Suslov, A. V. (2023) Effect of a transverse electric field on the resistance of thin films of the $Bi_{1-x}Sb_x$ (x = 0–0.12) system on mica. *Physics of Complex Systems*, 4 (2), 75–80. https://www.doi.org/10.33910/2687-153X-2023-4-2-75-80 EDN TFGFTE

СФЕРОЛИТОВАЯ МИКРОСТРУКТУРА ТОНКИХ ПЛЕНОК ЦТС

Пронин Владимир Петрович, Сенкевич Станислав Викторович, Елшин Андрей Сергеевич, Мишина Елена Дмитриевна, Пронин Игорь Петрович

Аннотация. В работе показано, что образование лучистой сферолитовой микроструктуры в тонких пленках цирконата-титаната свинца, полученных методом высокочастотного магнетронного распыления, сопряжено с формированием радиальных растягивающих механических напряжений, действующих в плоскости подложки, величина которых возрастает с увеличением линейного размера сферолитов. Это приводит к изменению параметра решетки перовскитовой структуры и появлению индуцированной поляризации, величина которой может существенно превышать спонтанную поляризацию.

Ключевые слова: тонкие пленки ЦТС, сферолитовая микроструктура, генерация второй оптической гармоники, механические напряжения, индуцированная поляризация

Для цитирования: Pronin, V. P., Senkevich, S. V., Elshin, A. S., Mishina, E. D., Pronin, I. P. (2023) Spherulitic microstructure of thin PZT films. *Physics of Complex Systems*, 4 (2), 81–87. https://www.doi.org/10.33910/2687-153X-2023-4-2-81-87 EDN VSFWYN